Journal of Sound and Vibration 439 (2019) 173–193

Contents lists available at ScienceDirect

Journal of Sound and Vibration

journal homepage: www.elsevier.com/locate/jsvi

# Aerodynamic noise reduction by plasma actuators for a flat plate with blunt trailing edge

Laith Al-Sadawi [a], Tze Pei Chong [a, *], Jung-Hoon Kim [b]

[a] Department of Mechanical and Aerospace Engineering, Brunel University London, Uxbridge, England UB8 3PH, United Kingdom
[b] Fluids and Thermal Engineering Group, University of Nottingham, Nottingham, England NG7 2RD, United Kingdom

ARTICLE INFO

*Article history:*
Received 30 August 2017
Received in revised form 17 July 2018
Accepted 15 August 2018
Available online 4 September 2018
Handling Editor: P. Joseph

*Keywords:*
Active control of aerodynamic noise
Vortex shedding

ABSTRACT

An experimental study of active control of the vortex shedding narrowband tonal noise radiated near the blunt trailing edge of a flat plate with elliptical leading edge was performed using three different configurations of the single dielectric barrier discharge (DBD) plasma actuators. These devices can produce electric winds in the tangential, downward and spanwise directions, respectively, near the blunt trailing edge. Acoustics and flow measurements were carried out simultaneously at Reynolds numbers between $0.75 \times 10^5$ and $4 \times 10^5$, based on the flat plate chord length, inside an aeroacoustic facility. The range of alternating-current (AC) input voltages to these plasma actuators was relatively low at $< 5$ kV. The "tangential" plasma actuator is not very effective in the suppression of vortex shedding tonal noise (maximum 1–2 dB reduction), although the spatial distribution of the wake coherent modes calculated from the proper orthogonal decomposition becomes more compact than that produced by the baseline plasma off case, resulting in a shift of the tone frequency to a higher value. The "downward" plasma actuator can suppress the vortex shedding noise almost completely at the tone frequency (about 15 dB reduction at input voltage of 4.2 kV). The mechanism is related to the induced plasma jet acting as a virtual barrier to inhibit the interaction between the upper and lower separating shear layers, and to delay the formation of the vortex shedding. The "spanwise" plasma actuator, which can project array of streamwise vortices into the wake and compartmentalise the vortex shedding across the span, demonstrated a more superior tonal noise reduction capability at low input voltage (about 12 dB reduction at 3.0 kV). It is found that the plasma-induced jet magnitudes between 9 and 10% and 7% of the freestream velocity for the downward and spanwise plasma actuators, respectively, are already sufficient to achieve an effective reduction of the vortex shedding tonal noise.


## 1. Introduction

The unsteady flow structure behind a bluff body or blunt trailing edge has been studied extensively due to its importance in many engineering applications. The separation of the free shear layer from the sharp corners of the blunt trailing edge, for example, can lead to formation of vortices that shed alternately from each side of the body. These coherent vortices along with the unsteady velocity field will produce a force loading that increases the aerodynamic drag. If the frequency of the vortex

* Corresponding author.
*E-mail addresses:* laith.al-sadawi@brunel.ac.uk (L. Al-Sadawi), t.p.chong@brunel.ac.uk (T.P. Chong), Jung-hoon.kim@nottingham.ac.uk (J.-H. Kim).

https://doi.org/10.1016/j.jsv.2018.08.029

**Nomenclature**

| | |
|---|---|
| $B$ | *width of the flat plate, m* |
| $C$ | *chord length of the flat plate, m* |
| $C_D$ | *drag coefficient that includes the mean $C_{D(\mathrm{mean})}$, and the fluctuating $C_{D(\mathrm{rms})}$ components* |
| $f$ | *frequency, Hz* |
| $f_{(input)}$ | *input frequency to the plasma actuators, kHz* |
| $H$ | *flat plate thickness, also the bluntness, m* |
| $l$ | *eigenvectors of the covariance matrix $C_{ij}$* |
| $U$ | *mean flow velocity of the nozzle jet, $ms^{-1}$* |
| $u,v,w$ | *velocity components in the streamwise, wall-normal and spanwise directions, respectively, $ms^{-1}$* |
| $x,y,z$ | *streamwise direction measuring from the blunt trailing edge, wall-normal direction and spanwise direction, respectively, m* |
| $\hat{u}$, $\tilde{v}$ | *plasma-induced jet velocity in the x-direction and y-direction, respectively, $ms^{-1}$* |
| $u_{rms}$, $v_{rms}$ | *root-mean-square of the velocity fluctuation in the streamwise and vertical directions, respectively, $ms^{-1}$* |
| $u_\infty$ | *velocity at the potential flow region above the wake (used in Eqs. 3 and 4), $ms^{-1}$* |
| $V_{(input)}$ | *input AC voltage to the plasma actuators, kV* |
| $y^+$ | *normalized wall-normal distance ($yu_\tau/\nu$), where $u_\tau$ is the friction velocity and $\nu$ is the kinematic viscosity* |
| $\Delta$SPL | *difference in sound pressure level between the baseline (plasma off), and control (plasma on) cases, dB* |
| $\lambda_i$ | *eigenvalue of the covariance matrix $C_{ij}$* |
| $\theta$ | *momentum thickness of the wake flow, mm* |
| $\Omega_x$, $\Omega_z$ | *Streamwise and spanwise vorticity, respectively, $s^{-1}$* |
| $\psi^{(i)}$ | *POD-eigenmode* |

shedding coincides with the natural frequency of the flow body, it could then induce structural instability and reduce the life-expectancy of many lift-generating bodies in the civil aviation and wind turbine industries.

The aeroacoustic problem of a bluff body or blunt trailing edge, i.e. the radiation of narrowband tone as a result of the bluntness-induced vortex shedding, represents a prominent issue that has hitherto received relatively less attention. More research efforts are therefore needed to mitigate this type of important noise source. Because the radiated aerodynamic noise is usually a by-product of the flow structure generated on the body, it is possible to apply control technique to stabilise the wake flow and, at the same time, reduce the level of noise radiation into the far field.

There are numerous studies that aim to control the unsteady flow behind blunt bodies by modifying or suppressing the coherent structures in the wake region, which could be achieved by either the passive or active flow control approaches. A general review of the passive flow control on the suppression of vortex shedding behind bluff body can be found in Choi et al. [1]. For example, one can use the splitter plate with different gap ratios behind the bluff body [2–6]. Roshko [6] demonstrated that vortex shedding can be completely suppressed behind a cylinder, thus resulting in a reduction of the base drag when splitter plate with length 5 times the cylinder diameter is attached at the aft region. Roshko also showed that varying the gap ratio of the splitter plate between 0 and 1.75 times the cylinder diameter will result in an extension of the shear layers to the downstream edge of the splitter plate. This modification of the wake structure is found to be able to prevent the entrainment of the outer flow to the base region. It is also shown by Liu et al. [7] that applying the porous coating on tandem cylinders can lead to stabilisation of the vortex shedding from the upstream cylinder. As a result, the impact of wake impingement with the downstream cylinder is reduced. They postulated that the modified flow field by the porous coating will eventually lead to reduction in the wake vortex shedding noise radiated from the upstream cylinder, as well as the interaction noise with the downstream cylinder. Using small element near the trailing edge of a rectangle cylinder at low Reynolds number, Chen et al. [8] found that these element successfully suppress vortex shedding and reduce the fluctuation in the lift and drag forces. Although many of these passive flow control methods are popular due to their simplicity and ease of implementation, they usually require geometrical modification or attachment of moving or fixed parts to the main body. As a result, they are not very versatile when the flow condition can change considerably over a short period of time.

The improvement in control and electrical technologies in the last few decades encourages the development of the active flow control. The miniaturisation of the actuators also means that very little parasite drag is produced when they are attached to the flow body. The active flow control both in the open-loop and closed-loop modes can adapt to various flow conditions effectively, thus allowing the user to switch them on and off easily. To attenuate the bluntness-induce vortex shedding, one could seek to prevent the cross-talk between the two separated shear layers, as well as to promote a faster break-up of the coherent structure in the near wake region. Using steady suction and blowing, Henning and King [9] showed that the spanwise coherence of the vortex sheet from a D-shaped elongated body could be modified. For the same set up, piezo-fluidic actuators were utilised to control the stability of the free shear layer. Stalnov et al. [10] studied a closed-loop feedback control of a D-shaped cylinder wake. Based on the proper orthogonal decomposition modeling, it was demonstrated that the body-

mounted sensors and Piezo-electric fluidic actuators were nearly collocated. Despite the robustness and flexibility for the active control, some disadvantages still persist. These include the complexity of the control system, the need for external power source and the increased overall weight associated with the actuator system.

More recently, many studies have focused on a promising active flow control technique that could alleviate some of the disadvantages described above. The dielectric barrier discharge (DBD) plasma actuator is simple, robust, light-weight, high frequency in response and low-power consumption in the unsteady operation mode. It has been demonstrated in many studies that placing single or multiple DBD plasma actuators close to the separation point of an aerofoil can prevent the boundary layer separation and increase the lift coefficient [11,12]. Post and Corke [11] showed that the plasma actuator can also prevent flow separation and the formation of dynamic stall vortex for an oscillating aerofoil. More interestingly, reduction of the turbulent boundary layer skin friction can be achieved by spanwise actuation of the DBD plasma actuators in the same control principle as the mechanical spanwise oscillation [13]. Huang and Zhang [14], Thomas et al. [15] and Huang et al. [16] are examples of the pioneering researchers who extend the plasma actuators in the aeroacoustic field, and successfully demonstrated that it can be an effective device to control the aerodynamic noise.

Under a specific Reynolds number regime, flat plate with a sufficiently blunt trailing edge can amplify the spanwise vorticity of the separated shear layer, roll up the shear layer and generate vortex shedding in the wake. Using several configurations of plasma actuators, Nati et al. [17] demonstrated that a downward plasma actuation can suppress the vortex shedding effectively. The mechanism is related to the production of a streamwise jet to prevent the cross-talk between the separating shear layers. The streamwise jet also increases the momentum and stability in the wake region. In Nati et al.'s experiment, the maximum freestream velocity is about 10 $ms^{-1}$ and the boundary layers generated on the plate surface were predominantly laminar.

It is known that a flat plate with a sufficiently "blunt" trailing edge, similar to the one used by Nati et al. [17], can generate vortex shedding in the wake which will then radiate high amplitude, narrowband tonal noise into the far field. They focus entirely on the fluid dynamics aspect of the flow field which was subjected to the use of DBD plasma actuators to control the bluntness-induced vortex shedding. However, the effect on the far field narrowband tonal noise has not been examined. The current paper attempts to fill this gap in the literature where three main objectives are defined. The first is to combine the flow and acoustical investigations for the use of DBD surface plasma actuators to suppress the vortex shedding in the wake, and at the same time to examine and quantify the level of reduction for the far field narrowband tonal noise. Second, the control strategy adopted by Nati et al. [17], which is to disrupt the communication between the separated free shear layers on both sides, or to add flow momentum into the recirculation region directly, would understandably require a high level of voltage input to feed the plasma actuators (typically at 18 kV peak-to-peak, or 9 kV effective voltage) so that a plasma-induced jet with reasonably large velocity magnitude can be produced. The current paper will investigate whether a much lower voltage input (e.g. < 5 kV) to the same configuration in the plasma actuator (i.e. the downward actuation) can trigger another control mechanism which will be as effective as those under high level of input voltage for the suppression of the vortex shedding and reduction of the far field narrowband tonal noise. Third, all the different configurations of plasma actuator investigated by Nati et al. [17] exclusively produce streamwise travelling waves that interact with the downstream wake usually dominated by a strong spanwise vorticity field. On the other hand, it is possible to design a new plasma actuator configuration such that it can produce array of counter-rotating streamwise vortices in the same manner as the vortex generators (e.g. Huang and Zhang [14]). The current paper will investigate whether these plasma-induced streamwise vortices can continue to propagate downstream and counteract with the dominant spanwise vorticity field in the wake, thereby inhibiting the formation of the vortex shedding and reducing the far field aerodynamic noise.

## 2. Experimental setup and analysis technique

### 2.1. Aeroacoustic wind tunnel facility and the test model

Both the acoustic free field and near field flow measurements were conducted in the aeroacoustic wind tunnel at Brunel University London. This facility includes an anechoic chamber with dimension of 4 m × 5 m × 3.4 m. A centrifugal fan positioned outside the anechoic chamber is used to generate the air flow, which will be acoustically treated by a 10 m long silencer located on the roof outside the chamber. After leaving the silencer, the moving air will continue to propagate inside an almost constant-area duct system that comprises two 90-degree bends and several flow straightening devices (honeycombs and woven-wire gauge screens), and eventually enter the anechoic chamber. The flow is then accelerated through a nozzle of high area ratio (25:1) inside the chamber. The exit nozzle is rectangular shape of 0.1 m (height) and 0.3 m (width). The maximum jet speed that can be produced by this facility is about 80 $ms^{-1}$. In the current experiment, the effectiveness of the plasma actuators on the suppression of the flat plate aerodynamic noise is investigated at jet speed, $7.5 \leq U \leq 40$ $ms^{-1}$, which corresponds to chord-based Reynolds number between 0.75 and $4 \times 10^5$.

As shown in Fig. 1, the flat plate has a chord length $C = 0.15$ m and width $B = 0.3$ m. One end of the flat plate has an elliptical shape that serves as the leading edge to facilitate a smooth entry of the incoming flow. Another end of the flat plate is truncated that leaves a sharp bluntness, $H = 0.006$ m. The flat plate was fixed by two side plates extending from the nozzle, and was placed at zero incidence with relative to the jet flow direction. The flow across the flat plate is predominantly two-dimensional. Unlike Nati et al. [17], the boundary layer on the flat plate was artificially tripped into turbulent flow in the current study. The vortex shedding produced by the blunt trailing edge is therefore originated from the roll up of the

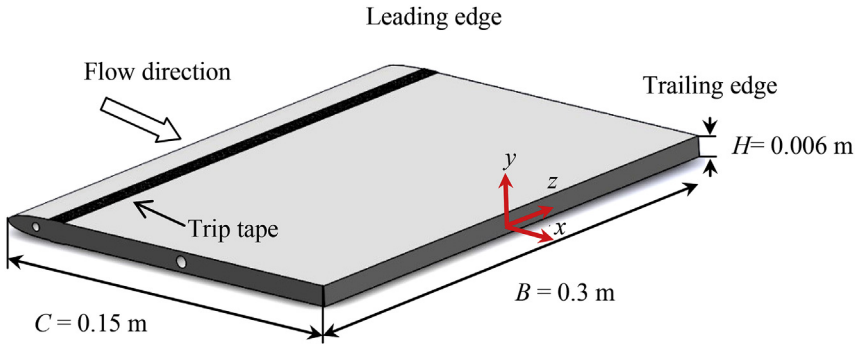


**Fig. 1.** Flat plate model with blunt trailing edge investigated in the current study.

turbulent shear layer near the blunt trailing edge. The boundary layer tripping was performed at both the upper and lower sides of the flat plate at 15 mm downstream of the leading edge using rough sandpapers.

As shown in Fig. 1, the *x*, *y* and *z*, refer to the streamwise, heightwise and spanwise directions, respectively, throughout the paper. $x = 0$ is located at the blunt trailing edge, where a positive *x* represents the distance downstream of the blunt face, and vice versa. It should be mentioned that $y = 0$ is located at the middle point of the flat plate thickness, not at the plate surface.

### 2.2. Configuration of the DBD plasma actuators

The DBD plasma actuators basically consist of two electrodes. One is exposed to the atmosphere in which high voltage is supplied from an alternating-current (AC) high-voltage power supply; and another electrode is grounded or encapsulated, which is usually covered by either a single or multiple layers of dielectric material (Teflon, Kapton or ceramic). The purposes of the dielectric material are to prevent arc-occurrence between the two electrodes, and to allow for discharge accumulation near the exposed electrode. When high AC voltage of $V_{(input)}$ ~ kV with typical sinusoidal waveform of $f_{(input)}$ ~ kHz is supplied, strong electric field is generated between the two electrodes. This leads to the creation of an ionised region that contains approximately equal number of ions and electrons [18]. A body force will then be generated as a result of the collision between the ions and neutral particles. This, in turn, produces an electric wind passing over as a surface jet parallel to the flow direction. High level of supplied voltage is usually required in order to produce the electric wind.

As illustrated in Fig. 2, three configurations of the plasma actuator were investigated in the current study. They are named according to the generated electric wind direction. The first is the actuator that generates a tangential electric wind, which is called the PA1. In this configuration, the plasma creates a body force near the electrode surfaces and draws the high momentum air from the freestream towards the wall near the edge to modify the characteristics of the shear layer. The second configuration (PA2) generates electric wind in the vertical direction along the blunt face of the trailing edge. This particular configuration is similar to the downward plasma configuration adopted by Nati et al. [17]. For the third configuration (PA3), a series of plasma actuators is aligned in the direction of the mean flow to produce spanwise travelling waves. The momentum coupling of the plasma ions by each actuator is initiated between a pair of exposed and ground electrodes. The dielectric material used throughout the experiment is the Kapton tape, which is known to have high dielectric strength. The material used for both the exposed and ground electrode is the copper tape. Note that both the PA1 and PA2 plasma actuators are situated adjacent to the blunt trailing edge, while the PA3 plasma actuators are located at $x = -4$ mm, i.e. away from the trailing edge in the upstream direction. As shown in Fig. 2, the spanwise spacing between each exposed electrode (edge-to-edge) is 9 mm, and the width of each exposed electrode is 6 mm. An AC power supply (MiniPulse 6) is used to provide the AC voltage to the electrodes. Subjected to the overall capacitance level of the plasma actuators, this power supply is capable of generating up to 60 kV peak-to-peak. A signal generator (LeCroy wave station) is used to produce a sinusoidal wave as an input signal to drive the voltage supply. The voltage range tested in the current study is $2.4 \leq V_{(input)} \leq 4.8$ kV.

### 2.3. Experimental instrument and flow field analysis techniques

The far field noise was measured by a ½-inch free field type pre-polarised condenser microphone (LarsonDavis 377B02). The microphone is situated at 1 m directly above the trailing edge at the mid span of the flat plate. A 16-bit analogue-to-digital card was used to sample the noise data at a sampling frequency of 44 kHz for 10 s. The sampled data were then windowed and the power spectral density (PSD) of 1 Hz frequency bandwidth was computed from a 1024 point Fast Fourier Transform (FFT).

The wake flow generated by the blunt trailing edge and their changes in the velocity properties as a result of the plasma flow control is studied by the glass Pitot tube, hot wire anemometry and Particle Image Velocimetry (PIV). The glass pitot tube, which has an inner diameter of 1 mm, was used to measure the near wake mean velocity profile at streamwise locations of $x = 1$ and 3 mm. The total pressure was measured by a differential pressure transducer that has a pressure sensitive range between 0 and 10 mbar (Sensortechnics HCXM010D6H). The reference pressure (static ambient pressure) was measured by

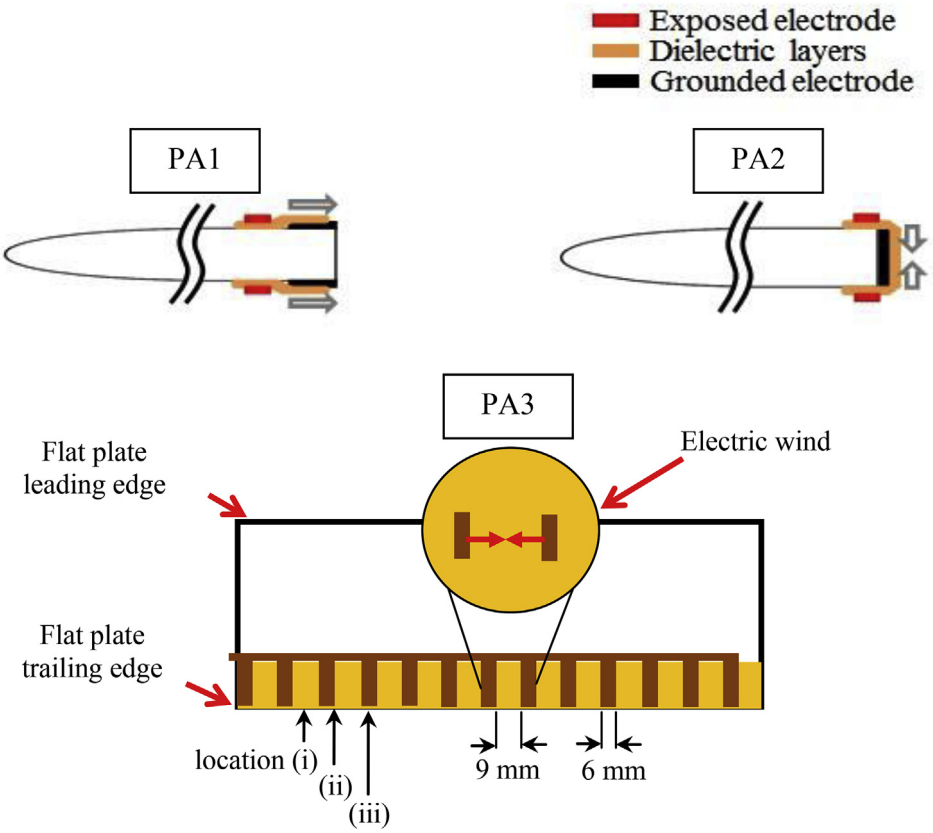


**Fig. 2.** The three plasma actuator configurations PA1, PA2 and PA3 (drawings are not to scale).

another tube that was positioned not far from the trailing edge but away from the jet. Note that the hot wire probe was not used for the near wake measurement in order to avoid electrical arching between the plasma discharge and metal prongs of the hot wire probe. The hot wire was instead used to measure the instantaneous velocity profile and fluctuating velocity power spectral density at $x = 25$ mm. The hot wire is the DANTEC 55P11 type and it is connected to a constant temperature anemometer (DANTEC 55M01). The glass Pitot tube and hot wire probe were connected to a two-directional traverse system that has an accuracy of 0.01 mm in both directions.

The velocity field near the blunt trailing edge of the flat plate was also measured by the PIV technique. The PIV system includes a source that generates a double pulse laser beam (Litron® Nd:YAG-Laser) with maximum output energy of 200 mJ. The laser beam has a diameter of 5 mm that can be expanded through a set of lenses. The maximum pulsing frequency is 15 Hz. A CCD camera (FlowSense EO 2M) is used to capture the images of the flow domain at 44 frames/second with an output resolution of $1600 \times 1200$ pixel on size of 7.4 μm. Polyethylene glycol (PEG) oil was used as seeding fluid because of its good reflection characteristics at high laser intensities. The oil droplet has an average diameter of 2 μm which was seeded via a pressurised oil chamber (Dantec high volume liquid droplet seeding generator) and injected to the anechoic chamber. Conventional cross-correlation algorithm was used on $32 \times 32$ pixel grid to calculate the velocity vectors from the peak correlation of a group of particles. The average velocity was computed by averaging approximately 540 images of the instantaneous velocity distribution. Because of the shining surface of the exposed copper electrode, a certain level of laser reflection occurs near the plasma actuators, which contaminates the PIV results at the near wall region.

The PIV experiment focuses on two types of measurement plane. The first is in the $x$–$y$ plane where the camera was placed perpendicularly to the streamwise direction for both the PA1 and PA2 plasma actuators. Under this setting, various instantaneous and time-averaged flow quantities can be measured. These include the mean velocities $u$, $v$, spanwise vorticity $\Omega_z = (\partial v/\partial x - \partial u/\partial y)$ and the energy-based coherent modes (to be discussed in the proper orthogonal decomposition). Note that $u$, $v$ and $w$ are the velocity components in the streamwise, vertical and spanwise directions, respectively. The second is in the $z$–$y$ plane, where the camera was placed at $x = 1.3$ m behind the blunt trailing edge and its line of sight is configured to be against the main flow direction. This configuration allows the investigation of the streamwise vortices generated by the PA3 plasma actuator in terms of the streamwise vorticity $\Omega_x = (\partial v/\partial z - \partial w/\partial y)$. Because the PIV system is operated in double frame mode for the image capturing, it is important to ensure that majority of the smoke particles remain within the

thickness of the laser plane between the pulses under this particular viewing angle. Therefore the PIV measurement in the $y-z$ plane was only performed at the lowest jet speed at $U = 7.5\ \mathrm{ms}^{-1}$, where the accuracy of velocity deficit measured at the wake region will even be better. A special tripod system was setup to hold the camera securely to minimise the flow-induced vibration on the camera.

The proper orthogonal decomposition (POD) is a mathematical linear procedure that can be used to extract the different energy modes from an ensemble of signals [19]. In the current study, the snapshots of the two-dimensional velocity fields, $\boldsymbol{v} = (x, y, t_n)$, where $n = 1, \ldots, N$, and $t_n$ is the time of the snapshot, are acquired by the PIV. $N$ is the total number of snapshots, which can be used to construct a covariance matrix $C_{ij}$:

$$C_{ij} = N^{-1}\left(\boldsymbol{v}(x, y, t_i), \boldsymbol{v}(x, y, t_j)\right), \tag{1}$$

where $i, j = 1, \ldots, N$.

A corresponding eigenvalue problem can be solved:

$$C_{ij} l^{(i)} = \lambda_i l^{(i)} \tag{2}$$

Since $C_{ij}$ is symmetric, it has $N$ real eigenvalues $\lambda_1 \geq \lambda_2 \geq \ldots \geq \lambda_N$ with the corresponding eigenvectors $\boldsymbol{l}^{(1)}, \boldsymbol{l}^{(2)}, \ldots, \boldsymbol{l}^{(N)}$, where $\boldsymbol{l}^{(i)} = (l_1{}^{(i)}, l_2{}^{(i)}, \ldots, l_N{}^{(i)})^t$. The POD analysis gives the basis to re-produce the velocity field by the modal decomposition as a linear combination of

$$\psi^{(i)}(x, y) = \sum_{n=1}^{N} l_n^{(i)}\, \boldsymbol{v}(x, y, t_n), \tag{3}$$

where $\psi^{(i)}$ $(i = 1, \ldots, N)$ represents the POD-eigenmodes. The ordering of both the eigenvalues and eigenvectors ensure that the first mode, which is of the highest energy mode, represents the large scale coherent structure in the wake region.

## 3. Discussion of results

As described in Section 2.2, three plasma actuator configurations (PA1, PA2 and PA3) were investigated individually for their ability to suppress the bluntness-induced vortex shedding and reduce the far field narrowband tonal noise. The performance of each plasma actuator can be influenced by many factors such as the dielectric/electrode materials, dimension and thickness, the gap distance between the exposed and ground electrodes, and the input AC voltage that can be driven by different types of frequency waveform. Because the main aim of the current work is to assess the effectiveness of the surface plasma technique in the aeroacoustic field, the level of aerodynamic noise reduction will be used as a basis for the determination of the optimum combination of the above operating parameters. Once this has been determined, the same combination will be implemented throughout the remaining of the experiment.

After the optimisation, Table 1 summarises the final geometrical specification and the operating range of the plasma actuator system for the PA1, PA2, and PA3. The only variables associated with the experiment are the level of input voltage ($V_{(input)} = 2.4–4.8$ kV) and the driven frequency ($f_{(input)} = 7$ and 8 kHz). Another important geometrical specification is the number of layers for the dielectric film near the trailing edge. In order to prevent the leakage of electrical current between the exposed and ground electrodes, it is preferable to use sufficient number of layers for the dielectric film. However, too many layers of the dielectric film will artificially thicken, as well as inadvertently introduce a geometrical step near the trailing edge. Therefore it is important to ensure that the chosen number of layers for the dielectric film can satisfy both the criteria described above.

The optimal aeroacoustic performance versus the overall thickness of the dielectric film, henceforth, can be identified from the Overall Sound Pressure Level (OASPL). This value is calculated by integrating the acoustic pressure fluctuation over a finite frequency range that corresponds to the bluntness-induced vortex shedding tonal noise at $U = 7.5\ \mathrm{ms}^{-1}$ (between 176 and 317 Hz). The examination focuses on the difference in the OASPL level between the "plasma off" case and the "plasma on" case for different layers of dielectric film. It is found that 5 layers of dielectric film not only offer a better guarantee to isolate the electrical current leakage between the exposed and ground electrodes, but also represent an optimum choice in terms of the aerodynamic noise reduction. The overall thickness of 5 layers of dielectric film is about 0.125 mm, which is equivalent to

**Table 1**
Geometrical and operational specifications of the plasma actuators.

| Parameter | PA1 | PA2 | PA3 |
|---|---|---|---|
| Exposed electrode (length and width) | 280 and 6 mm | 280 and 6 mm | 15 mm and 6 mm |
| Ground electrode (length and width) | 280 and 10 mm | 280 and 6 mm | 280 and 10 mm |
| Dielectric thickness | 0.125 mm | 0.125 mm | 0.125 mm |
| Applied voltages and frequencies | 2.4–4.8 kV and 7–8 kHz | | |
| Applied signal shape | Sinewave | | |

$y^+ = 3.75$ near the blunt trailing edge (note that the friction velocity is obtained by the Clauser method from the measured turbulent boundary layer velocity profile near the trailing edge, without the dielectric film). This value is well within the viscous sublayer of a turbulent boundary layer. Therefore using 5 layers of the dielectric films is not expected to alter the structure of the turbulent boundary layer considerably in the present case.

### 3.1. Overview of the hydrodynamic fields

Before the impact of the plasma actuators on the aerodynamic noise is discussed, this sub-section will first address the different hydrodynamic fields of the wake flow when subjected to the "plasma off" (baseline), and the "plasma on" PA1, PA2 and PA3 cases. Fig. 3 compiles the $x-y$ contour maps of the instantaneous spanwise vorticity ($\Omega_z$), as well as the POD mode 1 (i.e. contains the highest relative energy) for both the $u$ and $v$ velocity components, respectively. Because of the laser light reflection, the velocity field at the vicinity of the blunt trailing edge is not resolved well by the PIV. Therefore in the presentation the nearest streamwise location with respect to the blunt trailing edge shown in Fig. 3 is at $x/H \approx 0.3$.

For the "plasma off" case, the instantaneous $\Omega_z$ contour clearly demonstrates the presence of wake vortex shedding that starts to form at relatively close proximity to the blunt trailing edge, at $x/H \approx 2$ (this is also confirmed in the time-averaged $\Omega_z$ contour, to be presented later). For the most dominant POD mode in $u$, one notices the anti-symmetry of the streamwise velocity component across the top and bottom half of the blunt edge, which is then accompanied by an alternating pattern when propagating downstream in the wake. These features represent the footprint of a vortex shedding phenomenon since it will alternatively increase and decrease the streamwise velocity components in both the streamwise and normal directions. The most dominant POD mode for the $v$ velocity component is symmetric in the normal direction, but again exhibiting an alternative pattern in the streamwise direction. Both the eigenmodes in $u$ and $v$ are correlated as it can be observed that the $v$-modes always embed between two consecutive pairs of the $u$-modes. This demonstrates that the downwash and upwash phases of the shedding event are associated with minimal changes in the streamwise velocity. From both the instantaneous $\Omega_z$ and dominant POD modes, the wavelength of the successive shedding structure is found to be about $3.5H$. Assuming that the vortical structures propagate at 80% of the freestream velocity, it would result in a shedding frequency of 286 Hz. This characteristic frequency in the hydrodynamic field will be shown later to be closely associated with the acoustic frequency of the radiated tone noise.

Both the instantaneous $\Omega_z$ and dominant POD modes indicate that the vortex shedding event is still present despite the activation of the tangential wind by the plasma actuator PA1. However, the spacing between the modes for the $u$ and $v$ velocity components in the $x$-direction becomes more compact than the "plasma off" case. Now at $2.8H$, each shedding pair subjected to the same propagation rate of $0.8U$ would produce a higher shedding frequency of 357 Hz. The increased compactness of the modes in the spatial domain, and their implication to the aeroacoustic radiation will be discussed in Section 3.2. It is clear that a more drastic effect on the vortex shedding is achieved by the PA2 downward actuators, as well as the PA3 spanwise actuators. Note that locations (i) and (ii) for the PA3 spanwise plasma actuator refer to the centreline between each pair of the exposed electrodes, and the edge of the exposed electrode, respectively. For graphical illustration of these locations one can refer to Fig. 2. From the corresponding instantaneous $\Omega_z$ contours, there no longer exhibit a clear pattern of the coherent structures when the PA2 and PA3 plasma actuations. This is also manifested in the POD eigenmodes, where the dominant modes in $u$ and $v$ are now completely absence for both cases. Therefore, there is a strong indication that the PA2 and PA3 plasma actuators are more effective in the suppression of the vortex shedding, and possibly also the reduction of the far field narrowband tonal noise. A detailed analysis will be provided in Sections 3.3 and 3.4 for the PA2 and PA3 plasma actuators, respectively.

### 3.2. Plasma actuator PA1 – tangential actuations

The aerodynamic noise generated by the flat plate with a blunt trailing edge of $H = 6$ mm, and those subjected to the tangential plasma actuations (PA1), are presented in Fig. 4. The freestream velocity was set at $U = 7.5\ \mathrm{ms}^{-1}$ in accordance to the flow results presented in Section 3.1. Four different levels of $V_{(input)}$ between 2.4 and 4.2 kV, in a step of 0.6 kV, and two excitation frequencies $f_{(input)}$ of 7 and 8 kHz, represent a total of eight test cases in the investigation. In the noise spectra, all the frequencies are non-dimensionalised by the bluntness $H$ and the freestream velocity $U$.

For the baseline, "plasma off" case, a strong tonal peak at $fH/U \approx 0.24$ is clearly discernible. This characteristic value is close to the Strouhal number commonly observed in the hydrodynamic vortex shedding of bluff body. The associated dimensional acoustic frequency is equal to 300 Hz, which is indeed very close to the shedding frequency of 286 Hz identified earlier by the POD modes (see Section 3.1). Therefore the narrowband component in the acoustic spectra of Fig. 4 is clearly the by-product of the bluntness-induced vortex shedding of the flat plate. One of the main objectives of this work is to investigate whether the plasma actuators can be an effective control device to reduce or completely eliminate such prominent noise source.

All the sub-figures in Fig. 4 also contain noise spectra pertaining to the "plasma on" case. It should be mentioned that broadband noise increase can be observed at $fH/U > 0.3$ for all cases, including the other plasma actuator configurations PA2 and PA3. The noise increase is contributed by the self-noise generated by the plasma actuator, which is not an aerodynamic source.

Overall, the actuations of the PA1 plasma actuator do not appear to have a profound effect on the noise spectra at $fH/U < 0.3$ in Fig. 4, except for the largest $V_{(input)} = 4.2$ kV, and $f_{(input)} = 7, 8$ kHz cases where a moderate aerodynamic noise reduction of

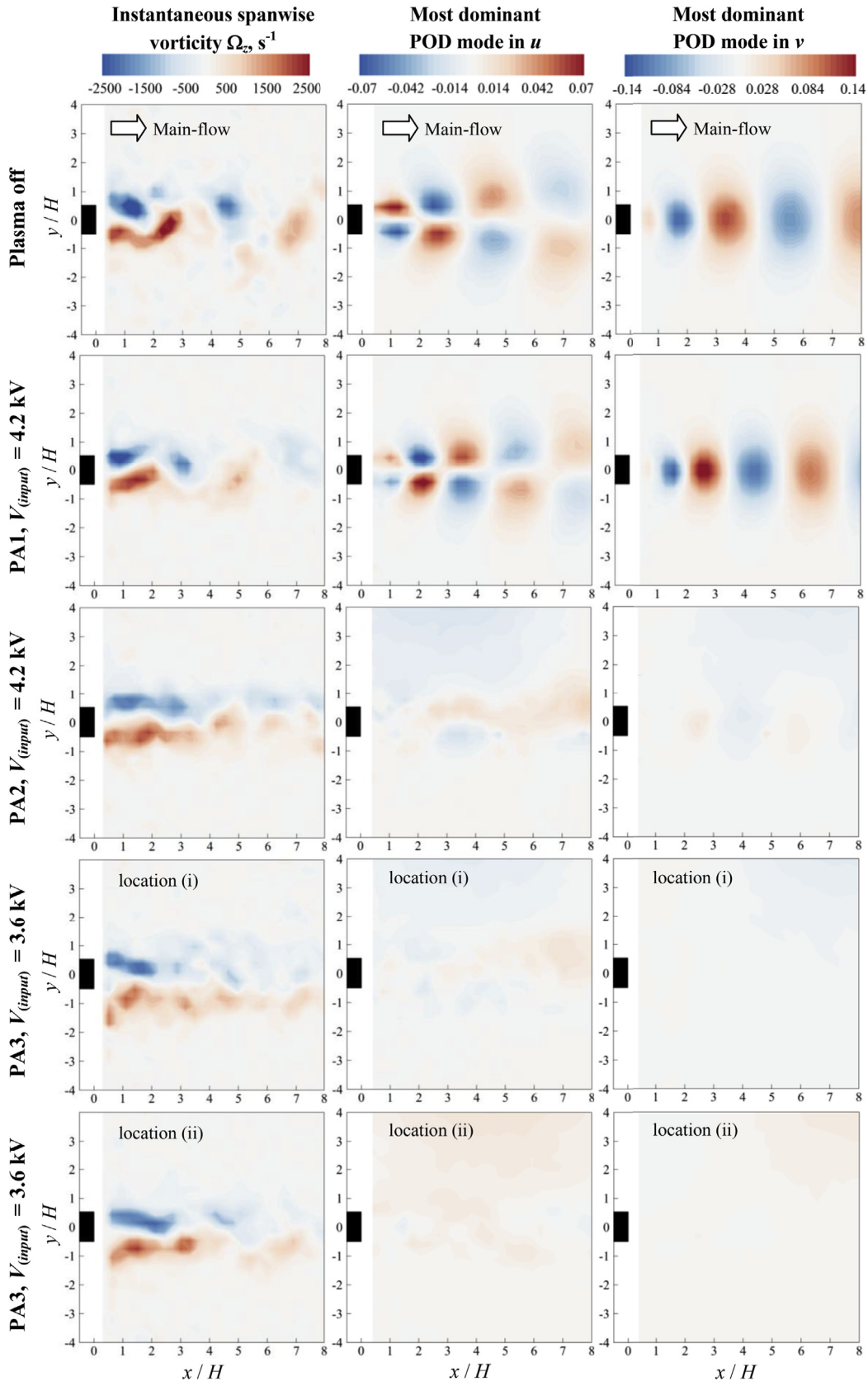


**Fig. 3.** Comparison of the instantaneous spanwise vorticity $\Omega_z$, and the most dominant POD modes in $u$ and $v$ for the different plasma actuators at $U = 7.5\ \mathrm{ms}^{-1}$.

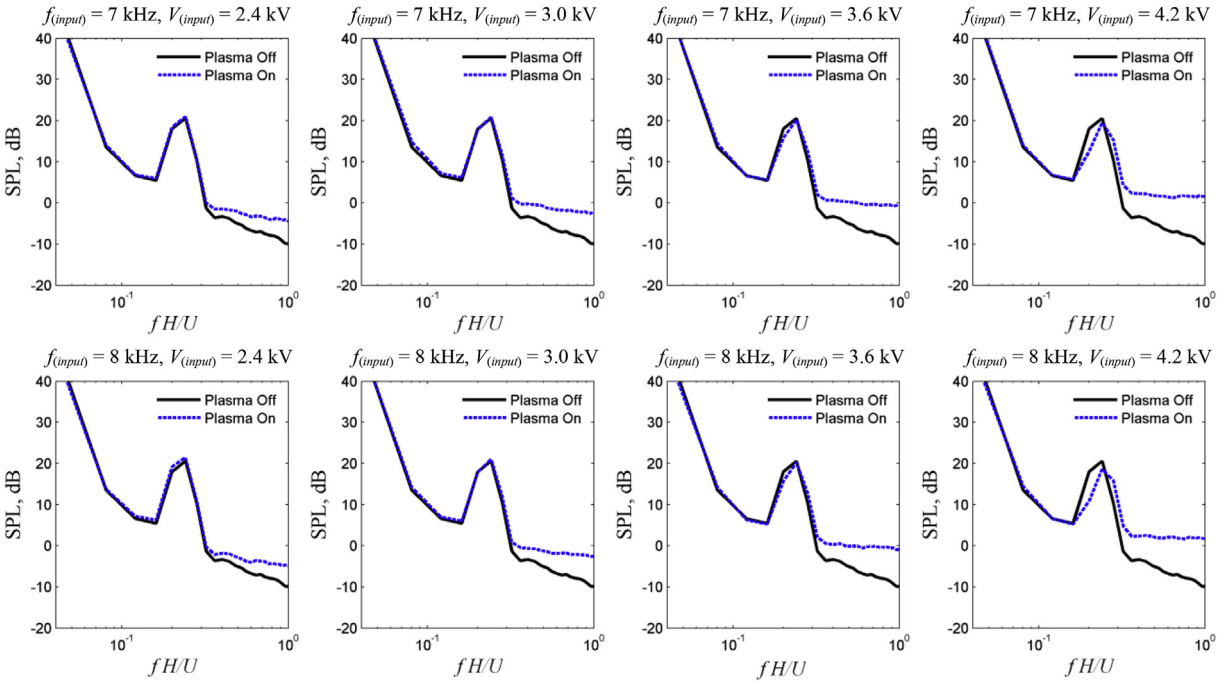


**Fig. 4.** Summary of the SPL spectra when the PA1 plasma actuator is operated at $f_{(input)} = 7$, 8 kHz and $V_{(input)} = 2.4$–4.2 kV at $U = 7.5$ ms$^{-1}$.

about 1–2 dB can be observed. This is also reflected in Fig. 3 for the corresponding instantaneous $\Omega_z$ and POD modes where both are qualitatively similar with the baseline "plasma off" case. However, the characteristic frequency of the reduced tonal noise appears to be shifted slightly to a higher value ($fH/U \approx 0.27$, or $f = 338$ Hz), which indicates that the induced plasma jet in the tangential mode has modified the wake vortex structure to a certain extent [12]. Indeed this is accurately manifested in Fig. 3 where the modified POD modes have resulted in a more compact wake vortical structure with a shedding frequency of 357 Hz.

Nevertheless, the time-averaged flow quantities subjected to the PA1 plasma actuation remain similar to the baseline "plasma off" case. For example, one can refer to Fig. 5 for the streamwise velocity fields for both the "plasma off" and PA1

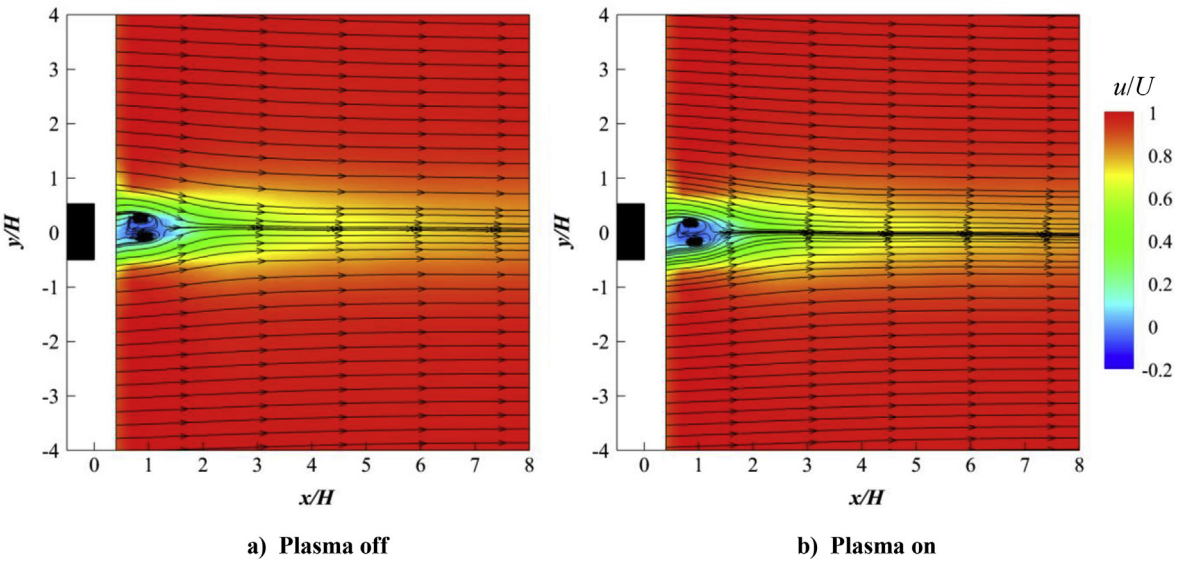


**Fig. 5.** Streamwise velocity fields generated by the PA1 plasma actuator at $U = 7.5$ ms$^{-1}$ when $f_{(input)} = 8$ kHz and $V_{(input)} = 4.2$ kV.

"plasma on" cases. In conclusion, although the PA1 tangential plasma actuator in the current setting can alter the shedding frequency slightly. It is not able to suppress the vortex shedding effectively.

It should be noted that a further increase of $V_{(input)}$ in the PA1 tangential plasma configuration has a potential to produce a stronger plasma jet, and in turn improve the level of reduction in the aerodynamic noise and possibly alter the wake coherent structures more significantly. However, as will be discussed later, the other two plasma configurations (PA2 and PA3) have demonstrated more superior level of reduction of the aerodynamic noise at $V_{(input)} \leq 4.2$ kV. Therefore further increase of the $V_{(input)}$ for the PA1 case is not reported in the current work.

Although the PA1 plasma actuators can only achieve a moderate level of aerodynamic noise reduction at the lowest $U = 7.5\ \mathrm{ms}^{-1}$, they were still investigated at higher freestream velocities $U$ for completeness. Fig. 6 shows the ΔSPL contours as a function of $U$ and $fH/U$. Note that the ΔSPL is the difference in SPL between the "plasma off" case and the "plasma on" case. A positive ΔSPL therefore denotes noise reduction against the baseline "plasma off" case, and the opposite is true. The upper and lower frequency limits for the narrowband vortex shedding tonal noise reduction are superimposed in the figures, which result in the appearance of three characteristic zones (*A*, *B* and *C*) in the $U$ and $fH/U$ domain. The zone *A*, which is largely characterised by ΔSPL ≈ 0, indicates that the plasma actuators have no effect on the aerodynamic noise at this particular frequency zone of low frequency. The frequency bandwidth associated with the reduction of the vortex shedding tonal noise (i.e. zone B), as a function of $U$, is bounded by two straight but inclined lines. The inclination indicates that a hydrodynamic length scale, which will vary with velocity, is more appropriate than a geometrical length scale to model the non-dimensional frequency range over which noise reduction by the plasma actuators is effective. The same characteristic also applies to the PA2 and PA3 plasma actuators, which will be discussed later. The level of noise reduction (i.e. ΔSPL > 0) increases slightly as the $V_{(input)}$ increases from 2.4 to 4.2 kV, but aerodynamic noise reduction is only quantifiable at $U \leq 15\ \mathrm{ms}^{-1}$. In zone *C*, the noise spectra at the low jet velocity region demonstrate the: (1) increase of broadband noise at high frequency, and (2) appearance of a distinct non-aerodynamic tone noise at frequency ≈ $f_{(input)}$, as well as several of its harmonics. Note that all these discrete frequencies do not exhibit the Strouhal-dependency associated with the plate bluntness. These non-aerodynamic noise sources are self-generated by the plasma actuators, with the largest level of tone occurs at the sub-harmonic frequencies of the $f_{(input)}$. The level of negative ΔSPL in zone *C* increases as the $V_{(input)}$ increases from 2.4 to 4.2 kV, but becomes less significant as $U$ increases. This is because the self-noise level generated by the plasma actuators, which is presumably only the function of the $V_{(input)}$, will be increasingly masked by the overall aerodynamic noise produced by the free jet and trailing edge of the flat plate model as $U$ increases. It is generally found that the plasma broadband self-noise in zone *C* will become insignificant (i.e. ΔSPL → 0) at $U \geq 20\ \mathrm{ms}^{-1}$, although the discrete tone at $f_{(input)}$ and several of its harmonics remain significant.

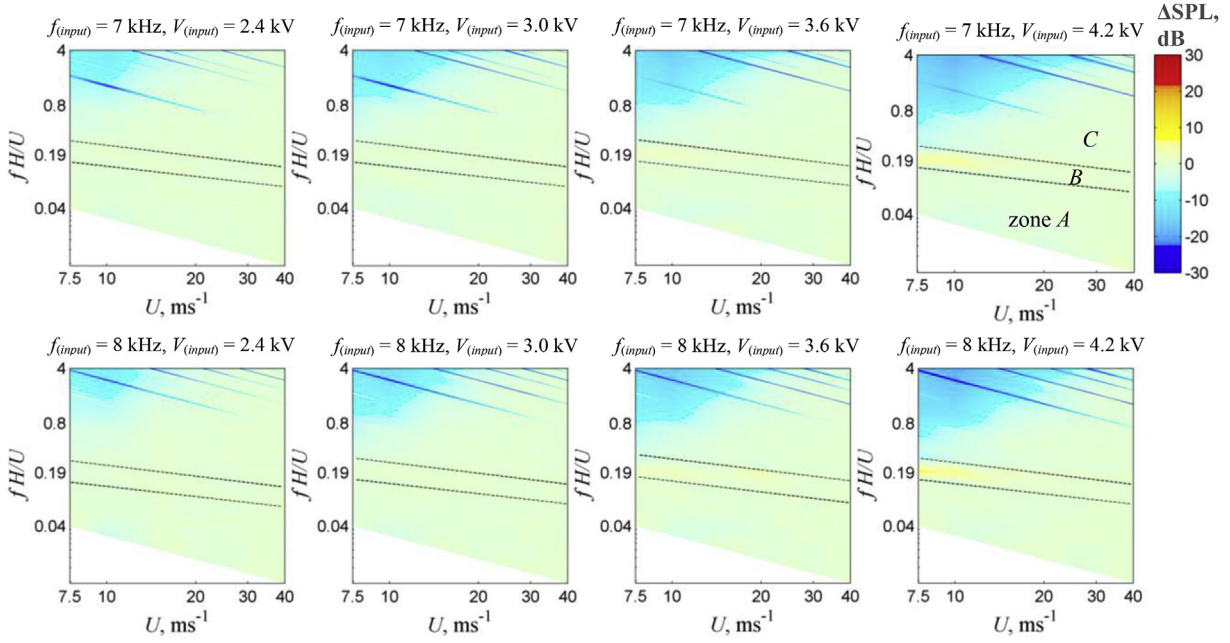


**Fig. 6.** Summary of the ΔSPL spectra when the PA1 plasma actuator is operated at $f_{(input)} = 7$, 8 kHz and $V_{(input)} = 2.4$–4.2 kV at $U = 7.5$–40 $\mathrm{ms}^{-1}$. The divisions for zones *A*, *B* and *C* are identical for all the contour maps.

### 3.3. Plasma actuator PA2 – downward actuations

The PA2 plasma actuator is designed to produce a "downward" electric wind at the blunt trailing edge. Before the discussion of aerodynamic noise reduction, the magnitude and characteristics of the ionic wind produced by this type of plasma actuator at the quiescent flow condition (i.e. $U = 0$) is shown in Fig. 7. The figure, which portrays a velocity field in the $x$–$y$ plane, demonstrates the induced velocity $\hat{u}$ downstream of the blunt trailing edge as produced by the plasma actuator PA2 when $V_{(input)} = 4.2$ kV and $f_{(input)} = 8$ kHz. It can be seen that, at $x/H = 0.5$, a jet with $\hat{u} \approx 1.8$ ms$^{-1}$ has been developed at the potential core, which then spreads uniformly as it develops downstream. Previously, the wake vortex shedding has been found to commence at $x/H > 2$ and undergo a complete cycle across a wavelength of $3.5H$. At $0.5 \leq x/H \leq 4.5$ in Fig. 7, the induced jet velocity decays from $\hat{u} \approx 1.8$ to 1.5 ms$^{-1}$. This represents only a 17% reduction in terms of the plasma jet velocity, which leads us to deduce at the beginning that the plasma-induced jet should be resilient enough to modify the wake flow directly in the non-quiescent condition, i.e. the main flow is present. However, as will be discussed in Section 3.3.1, another mechanism is actually responsible for the suppression of the vortex shedding and reduction of the narrowband tonal noise.

Note that the maximum induced velocity by the current PA2 downward plasma actuator is slightly less than those achieved by Nati et al. [17]. This is because they operated their plasma actuators at a higher $V_{(input)} = 9$ kV, at $f_{(input)} = 2$ kHz.

#### 3.3.1. Noise and flow measurements at $U = 7.5$ ms$^{-1}$

Under the current setting, the PA2 plasma actuator is capable of producing a reasonably strong induced jet. Next, its impact on the aerodynamic noise produced by flow passing over a blunt trailing edge will be examined. Fig. 8 shows the SPL spectra when subjected to different levels of $V_{(input)}$ (2.4–4.8 kV) and $f_{(input)}$ (7 and 8 kHz) to the plasma actuator PA2 at $U = 7.5$ ms$^{-1}$. The baseline "plasma off" case is also included in the spectra for comparison. The figure demonstrates an 8.3 dB reduction in the vortex shedding tonal noise for every 1 kV increase for the $V_{(input)}$. However, this linearity appears to be only valid at a certain voltage range, i.e. 2.4 kV $\leq V_{(input)} \leq$ 4.2 kV. It is observed that whilst there is little reduction in the vortex shedding tonal noise level at $V_{(input)} = 2.4$ kV, it can be reduced by 14.5 dB when $V_{(input)}$ is increased to 4.2 kV. When the $V_{(input)}$ is further increased to 4.8 kV, only a slight improvement of the vortex shedding tonal noise reduction of 15.2 dB is observed. Such a little difference in the level of vortex shedding tonal noise reduction between $V_{(input)} = 4.2$ kV and 4.8 kV, however, is only established at $U = 7.5$ ms$^{-1}$. Later it will be demonstrated that at $V_{(input)} = 4.8$ kV, the level of vortex shedding tonal noise reduction at higher $U$ can be much greater than that at $V_{(input)} = 4.2$ kV.

For consistency, the flow filed in Fig. 3 for the PA2 case underpinned by $V_{(input)} = 4.2$ kV and $f_{(input)} = 8$ kHz will be cross-referenced to the noise results in Fig. 8. The near complete suppression of the vortex shedding tonal noise under this plasma setting is well reflected by the relevant instantaneous $\Omega_z$ and dominant POD modes in Fig. 3.

For a like-for-like comparison in terms of the input voltage level, it is clear that the PA2 downward plasma actuator outperforms the PA1 tangential plasma actuator significantly in terms of the reduction in the vortex shedding tonal noise level. Next, the investigation focuses on the flow field near the blunt trailing edge when subjected to the downward actuation by the plasma actuator PA2. Under the combination of $V_{(input)} = 4.2$ kV and $f_{(input)} = 8$ kHz for the PA2 plasma actuators, and at the same $U = 7.5$ ms$^{-1}$ (same conditions as the results presented in Fig. 3), Fig. 9 presents the mean velocity contour $u/U$ in the

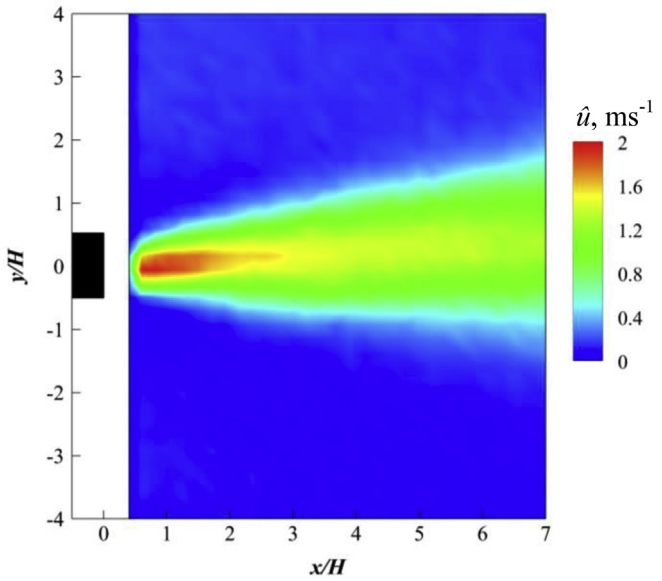


**Fig. 7.** Induced streamwise velocity field generated by the PA2 plasma actuator at quiescent condition (i.e. $U = 0$) when $f_{(input)} = 8$ kHz and $V_{(input)} = 4.2$ kV.

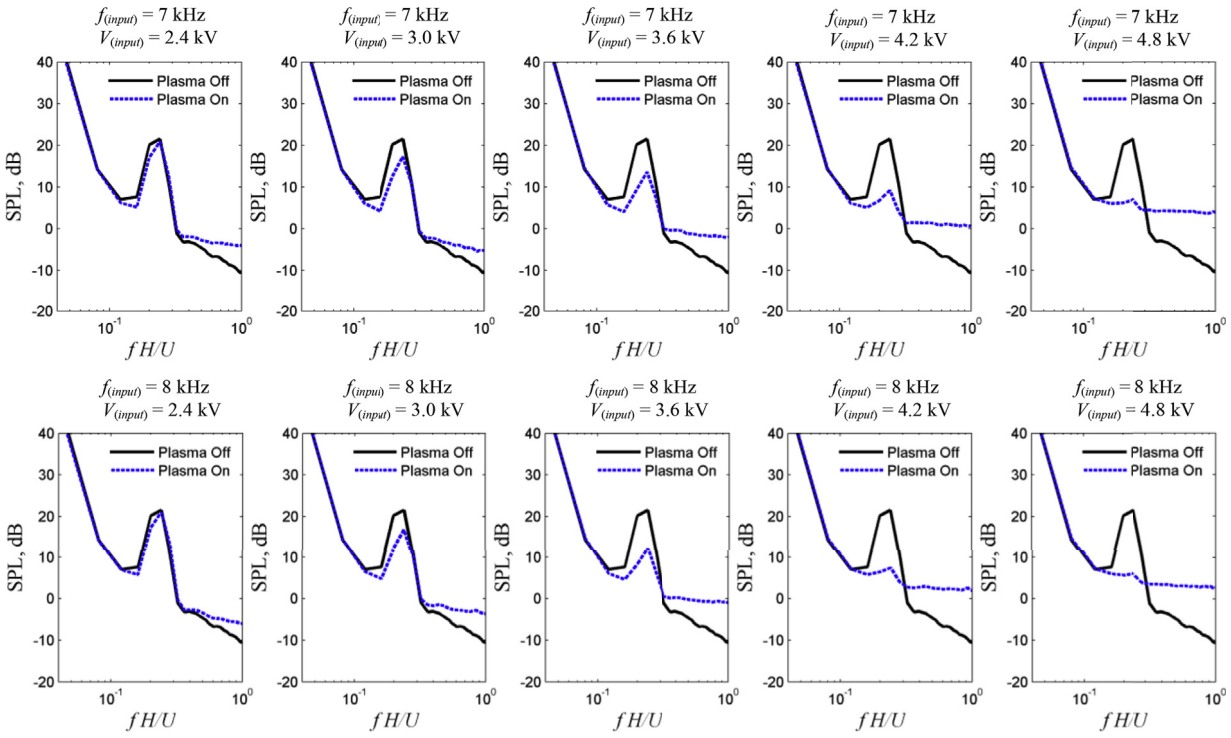


**Fig. 8.** Summary of the SPL spectra when the PA2 plasma actuator is operated at $f_{(input)} = 7$, 8 kHz and $V_{(input)} = 2.4$–4.8 kV at $U = 7.5\ \mathrm{ms}^{-1}$.

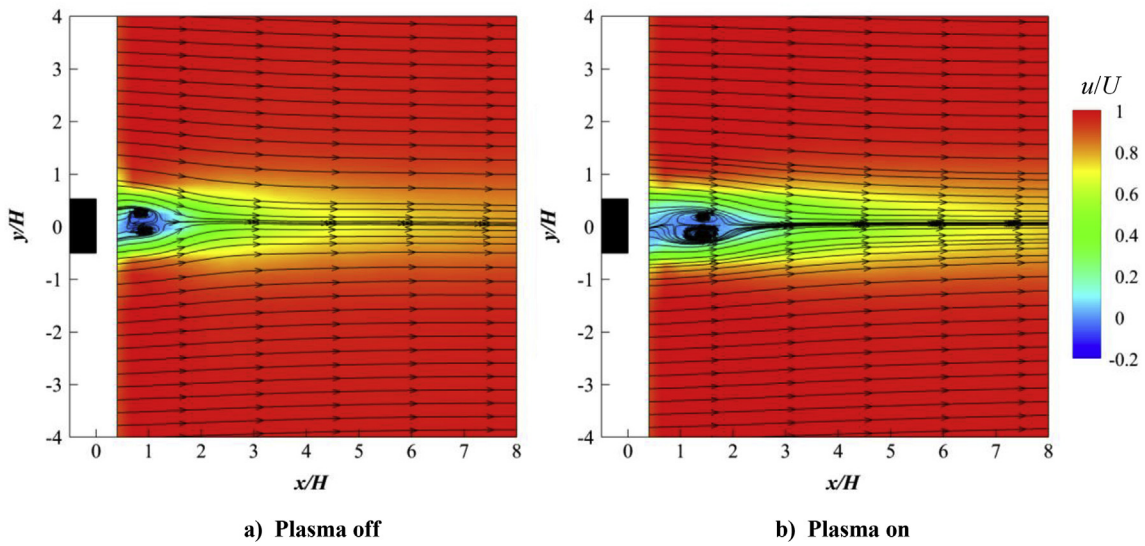


**Fig. 9.** Streamwise velocity fields generated by the PA2 plasma actuator at $U = 7.5\ \mathrm{ms}^{-1}$ when $f_{(input)} = 8$ kHz and $V_{(input)} = 4.2$ kV.

$x$–$y$ plane for the "plasma off" and PA2 "plasma on" cases. For the "plasma off" case, a re-circulating and non-convective region (i.e. $u/U \leq 0$) features prominently up to $x/H \approx 1.0$. At more downstream location, the separated shear layers from the flat plate blunt edges at the upper and lower sides, respectively, begin to interact with each other and form a convective shear flow where $u/U > 0$. For the PA2 "plasma on" case, the re-circulating region near the blunt trailing edge becomes larger in size, where the pocket is now elongated and shifted to $x/H \approx 1.5$, i.e. towards more downstream direction than the "plasma off" case.

The above results seem to contradict the convention where one would expect the induced air jet from the plasma actuators PA2, as demonstrated in Fig. 7 under the quiescent condition, to be able to inject momentum directly into the re-circulating

region, and as such, minimise the extent of the reversed flow. To investigate this further, a glass Pitot tube was used to measure the velocity profiles at $x/H = 0.17$ and 0.50 (correspond to $x = 1$ and 3 mm, respectively). Note that the velocity profile at $x/H = 0.17$ represents the very near wake region where the current PIV flow map cannot cover. The results for the "plasma off" and PA2 "plasma on" cases are presented in Fig. 10a and b. Note that $\hat{u}$ shown in the figure represents the plasma-induced jet velocity in the $x$-direction. It is well known that the total head measured by a Pitot tube in a reverse flow region will return zero value. If the velocity profile measured by a glass Pitot tube in Fig. 10a (i.e. at $x/H = 0.17$) is corroborated with the flow map measured by PIV in Fig. 9a and b, the predominantly zero value of $u/U$ for the "plasma off" case in Fig. 10a indeed corresponds to the re-circulating region. Interestingly, for the PA2 "plasma on" case at the same location of $x/H = 0.17$ in Fig. 10a, the velocity profile measured by the glass Pitot tube clearly exhibits a jet profile across the blunt face of the trailing edge. However, the maximum induced jet from the plasma actuator PA2 is found to be $\hat{u}/U = 0.05$, which gives $\hat{u} = 0.38\ \mathrm{ms}^{-1}$. This value is significantly lower than the $\hat{u} = 1.8\ \mathrm{ms}^{-1}$ at $x/H = 0.3$ (i.e. more downstream) under the quiescent location (Fig. 7). Furthermore, the plasma induced-jet seems to completely vanish at $x/H = 0.50$ in Fig. 10b. These results, which were obtained when there is main flow present, would contradict the more sustainable jet in the quiescent flow condition shown in Fig. 7 despite both were subjected to the same plasma settings and input AC voltage. The induced jet from the plasma actuator PA2 at the vicinity of the blunt face evidently fails to suppress the re-circulating region (see Fig. 9b). Therefore, question still remains of how exactly the induced jet by the PA2 plasma actuator could be so effective in the vortex shedding tonal noise reduction, as demonstrated in Fig. 8. Nevertheless, it is quite clear that the mechanism is not related to the direct injection of momentum to the wake such that the wake deficit can be minimised.

Next, the PIV mean velocity components are calculated to determine the time-averaged spanwise vorticity $\Omega_z$ of the flow field in the $x$–$y$ plane. Fig. 11a and b shows the time-averaged spanwise vorticity contours for the "plasma off" and PA2 "plasma on" cases, respectively. For the "plasma off" case in Fig. 11a, both sides of the blunt trailing edge produce two regions of spanwise vorticity of significance covering, approximately, $x/H \leq 2.5$. However, the two regions of spanwise vorticity of significance for the PA2 "plasma on" case extends to $x/H \leq 3.8$. Note that the spanwise vorticity of significance depicted in Fig. 11a and b, which is almost parallel to the direction of the mean flow, does not correspond to the shedding motion in the wake (which produces the tonal noise). This is because the repetitive rate of the PIV used here is lower than the vortex shedding frequency, hence it is unable to capture the unsteady motion (although the vortex shedding can still be shown quite clearly by the instantaneous $\Omega_z$ contour plots in Fig. 3). Rather, the time-averaged PIV data presented in Fig. 11a and b is related to the near wake, time-invariant separating shear layer as originated from the upstream boundary layer.

The Von Karman-type vortex shedding produced by the blunt trailing edge is originated from the roll up of the separating shear layer at some distance downstream of the blunt face. For the "plasma off" case, the relatively short length of the separating shear layer indicates that the vortex shedding is triggered close to the blunt trailing edge (at $x/H \approx 2$–2.5), after which the oscillation of the wake flow is sustained for a considerable distance to facilitate an effective radiation of narrowband tonal noise into the far field. For the PA2 "plasma on" case, the ionic jet produced by the plasma actuator does not seem to inject much momentum to the wake deficit, as demonstrated in Fig. 10. Rather, it acts like a virtual splitter plate to isolate the separating shear layers of the opposite sides and cut off the communication between them. As a consequence, the

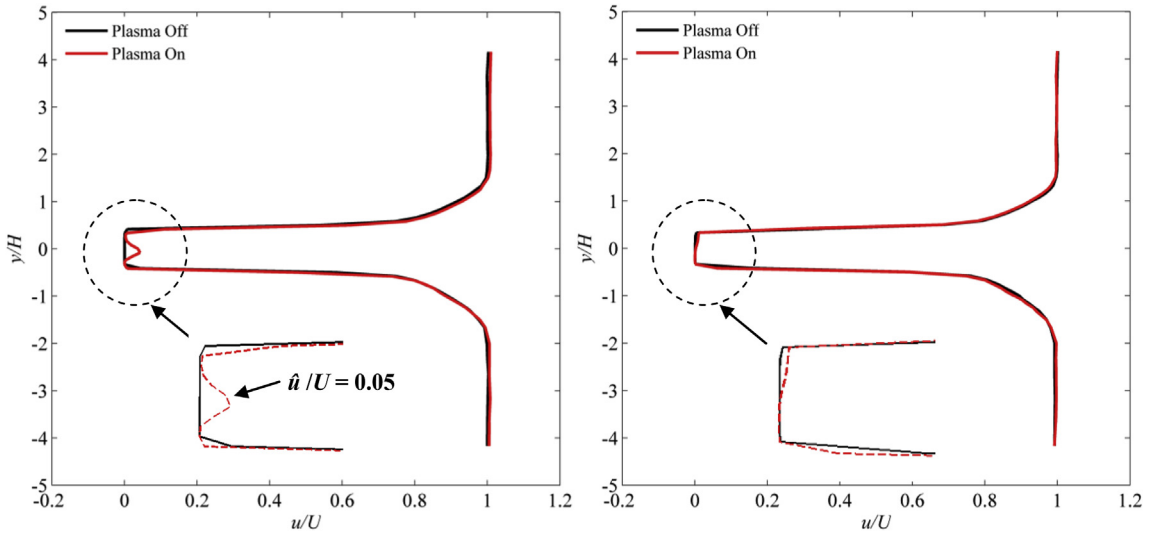


**Fig. 10.** Mean wake velocity profiles measured by the glass-Pitot tube at $U = 7.5\ \mathrm{ms}^{-1}$ when the PA2 plasma actuator is operated at $f_{(input)} = 8$ kHz and $V_{(input)} = 4.2$ kV.

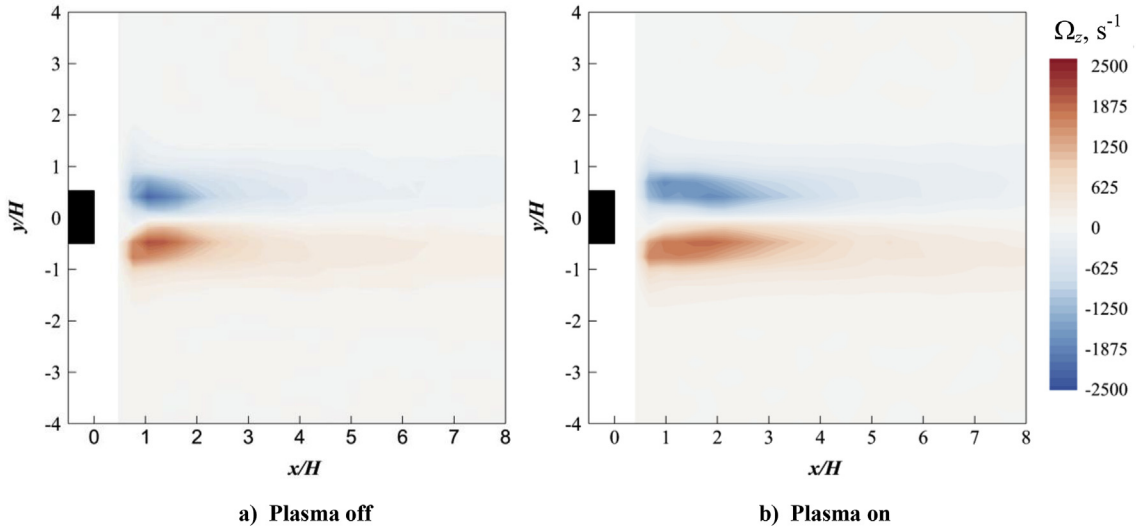


**Fig. 11.** Time-averaged spanwise vorticity fields generated by the PA2 plasma actuator at $U = 7.5\ \mathrm{ms}^{-1}$ when $f_{(input)} = 8$ kHz and $V_{(input)} = 4.2$ kV.

length of the separating shear layers is increased (Fig. 11b). The vortex shedding, if any, will be triggered at a more downstream location (at $x/H \approx 3.8$) which coincides with a much reduced energy level for the wake instability as per the POD analysis (Fig. 3). As a result, the level of the narrowband tonal noise radiation is also reduced significantly.

To verify the above interpretation, a hot wire probe is used to investigate the fluctuating velocity spectral density for both the "plasma off" and PA2 "plasma on" cases at $x/H = 4.17$ and $y/H = -1.17$, at $U = 7.5\ \mathrm{ms}^{-1}$. The reason to choose a relatively large $x/H$ and $y/H$ values for the measurement point is to ensure a safe distance between the hot wire probe and the plasma discharge so that electrical arching will not occur. Furthermore, the location of the hot wire at $x/H = 4.17$ is still behind the spanwise vorticity of significance in the wake produced by the PA2 "plasma on" case (Fig. 11b). As shown in Fig. 12 for the "plasma off" case, the reduced frequency for the narrowband peak of the fluctuating velocity spectral density occurs at $fH/U = 0.23$, which is very close to the narrowband tone observed in the acoustic spectra (see Fig. 8) under the same mean flow condition. This again confirms that the vortex shedding downstream of the blunt trailing edge is the main source for the tonal

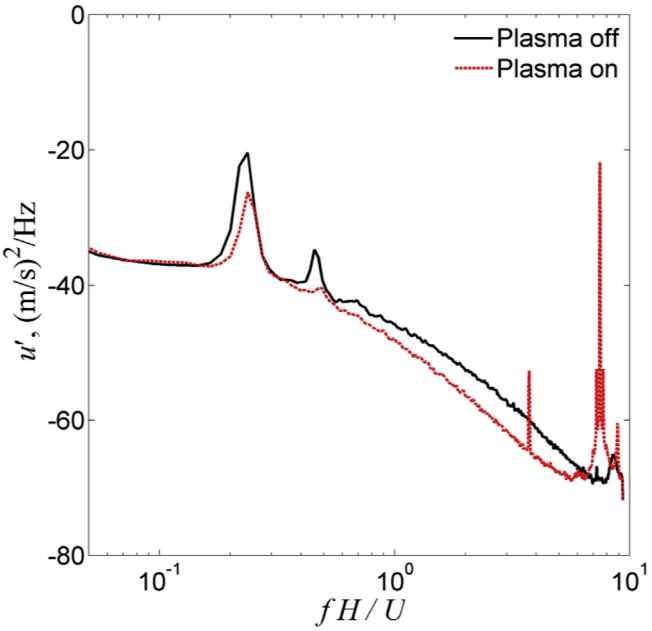


**Fig. 12.** Wake fluctuating velocity PSD measured by the hot wire probe at $U = 7.5\ \mathrm{ms}^{-1}$ when the PA2 plasma actuator is operated at $f_{(input)} = 8$ kHz and $V_{(input)} = 4.2$ kV. The measurement location is at $x/H = 4.17$ and $y/H = -1.17$.

noise radiation. When the PA2 plasma actuator is switched on at $V_{(input)} = 4.2$ kV and $f_{(input)} = 8$ kHz (the same input parameters as the PIV and glass Pitot tube tests), a reduction of the narrowband peak by about 10 dB can be observed in the fluctuating velocity spectral density. The harmonic of the primary narrowband peak that would otherwise be present in the "plasma off" case at $fH/U = 0.46$ almost disappears in the PA2 "plasma on" case. Although the results in Fig. 12 represent the far wake properties, it is expected that a similar, if not even larger level of reduction of the narrowband peak for the vortex shedding can also be achieved close to the blunt trailing edge when the PA2 plasma actuator is operated. The global reduction of the intensity or energy of the wake vortex shedding is thus manifested in the reduction of the narrowband tonal noise level.

*3.3.2. Mean and turbulent drag reductions by the PA2 plasma actuator*

It has now been established that the PA2 plasma actuator, when subjected to a modest level of input voltage, can almost completely suppress the vortex shedding tonal noise produced by a blunt trailing edge. One of the aerodynamic terms, namely the drag coefficient $C_D$, is now the subject of investigation here. Antonia and Rajagopalan [20] describe the drag of a circular cylinder, which can be determined from the wake velocity profiles of the mean and fluctuating components at less than 30 diameters downstream of the cylinder. This is a classical method to calculate the drag coefficient at near wake, but an assumption needs to be made *a priori* where the ambient pressure should already be established at the measurement points. The same principle is applied here where near wake of the flat plate blunt trailing edge can be used to calculate the mean and fluctuating component of $C_D$, given by $C_D = C_{D(\mathrm{mean})} + C_{D(\mathrm{rms})}$, respectively. For a unit span of the flat plate:

$$C_D = \frac{2}{C}\int_{-\infty}^{\infty}\frac{u}{u_\infty}\left(1-\frac{u}{u_\infty}\right)dy + \frac{2}{C}\int_{-\infty}^{\infty}\frac{(v_{rms})^2-(u_{rms})^2}{u_\infty^2}dy, \tag{4}$$

where $u_\infty$ is the freestream velocity at the measurement point, $C$ is the chord length of the flat plate, and $u_{rms}$ and $v_{rms}$ are the root-mean-square of the fluctuation velocity in the streamwise and vertical directions, respectively. The first and second terms on the right hand side of Eq. (4) represent the $C_{D(\mathrm{mean})}$ and $C_{D(\mathrm{rms})}$, respectively. Now, the momentum thickness of the wake, $\theta$, can be defined as:

$$\theta = \int_{-\infty}^{\infty}\frac{u}{u_\infty}\left(1-\frac{u}{u_\infty}\right)dy. \tag{5}$$

Therefore,

$$C_{D(\mathrm{mean})} = \frac{2}{C}\theta. \tag{6}$$

The momentum thickness of the wake can be calculated directly from the PIV data. The wake profiles for the analysis of the $C_D$ are examined at $2 \le x/H \le 4$. At $U = 7.5$ ms$^{-1}$, the $C_{D(\mathrm{mean})}$ calculated for the "plasma off" case is 0.0477 ±0.002. For the PA2 "plasma on" case when $V_{(input)} = 4.2$ kV and $f_{(input)} = 8$ kHz, the $C_{D(\mathrm{mean})}$ is 0.0369 ± 0.0024. The "plasma off" and PA2 "plasma on" cases produce the $C_{D(\mathrm{rms})}$ of 0.0034 ± 0.0003 and -0.0008 ±0.0003, respectively. The negative value for the $C_{D(\mathrm{rms})}$ for the "plasma on" case, although negligibly small, is caused by a much faster decay of the $(v_{rms}/u_\infty)^2$ term than the $(u_{rms}/u_\infty)^2$ term, which is also a manifestation of a very significant suppression of the vertical fluctuation of the vortex shedding by the PA2 plasma actuator.

*3.3.3. Tonal noise reduction at higher mean flow velocities*

Up to now, it has been demonstrated that the PA2 plasma actuator is very effective in the suppression of the narrowband vortex shedding tonal noise (as well as the mean and turbulent drag) at $U = 7.5$ ms$^{-1}$, which at this freestream velocity would deliver the largest ratio between the plasma jet velocity, $\hat{u}$ and the freestream velocity, $U$ of $\hat{u}/U = 0.24$ for the setting when $V_{(input)} = 4.2$ kV where the corresponding maximum $\hat{u}$ is about 1.8 ms$^{-1}$ (determined from Fig. 7). Unlike the value of $\hat{u}/U = 0.24$ quoted here which represents an upper-limit, it will be interesting to investigate the lower-limit of $\hat{u}/U$ where the suppression of the vortex shedding tonal noise could still be effective. Using the same range of $V_{(input)}$ (2.4–4.8 kV) and $f_{(input)}$ (7, 8 kHz), Fig. 13 shows the ΔSPL contour maps as a function of the $U$ (7.5–40 ms$^{-1}$) and $fH/U$. Similarly, a +ΔSPL represents noise reduction, and the opposite is true. These contour maps are also characterised by three zones *A*, *B* and *C*, similar to the format previously adopted in Fig. 6.

The level of +ΔSPL achieved by the PA2 plasma actuator on the narrowband vortex shedding tonal noise is manifested in zone *B*. It is found that the $f_{(input)}$ at either 7 or 8 kHz for the plasma actuator produces little difference in the noise reduction performance. At higher $V_{(input)}$, however, the +ΔSPL level becomes more significant and extends to higher $U$. More importantly, the results show that the upper-limit for $U$ that still achieves ΔSPL > 0 will increase as $V_{(input)}$ increases. For example, significant tonal noise reduction can still be achieved at $U \approx 22$ ms$^{-1}$ when $V_{(input)} = 4.8$ kV; at $U \approx 19$ ms$^{-1}$ when $V_{(input)} = 4.2$ kV; at $U \approx 16$ ms$^{-1}$ when $V_{(input)} = 3.6$ kV, and so on. Based on the above relationship, and assuming that the generation of $\hat{u}$ is a linear function of $V_{(input)}$, it is found that $0.09 \le \hat{u}/U \le 0.10$ represent the minimum ratio between the plasma jet and the freestream velocity for which an effective reduction of the vortex shedding tonal noise can be achieved at

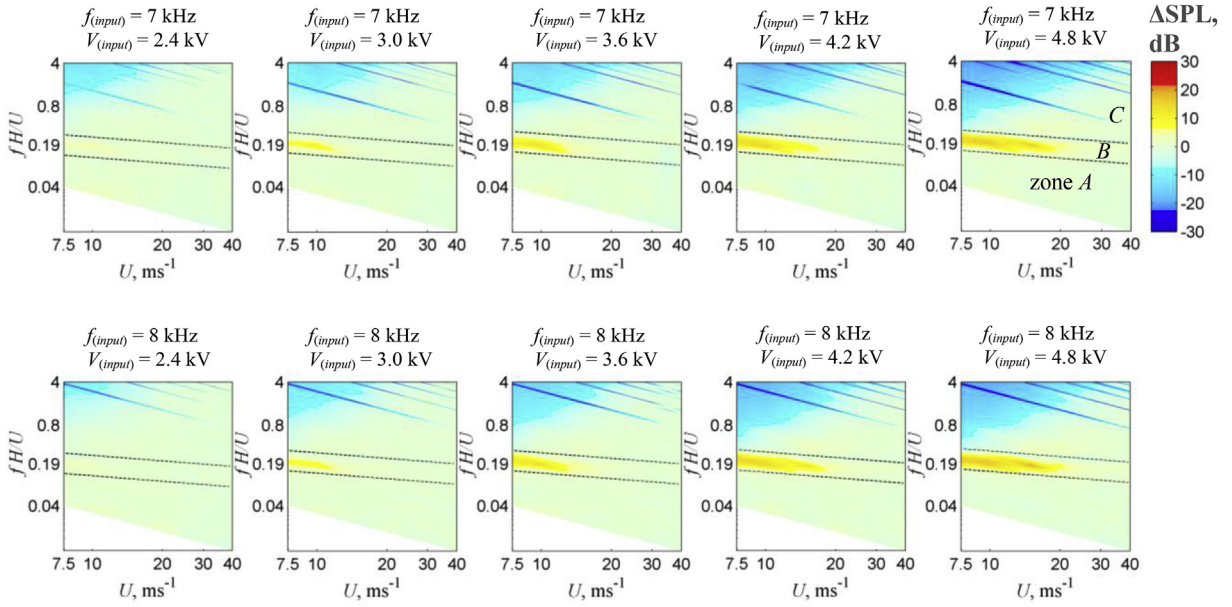


**Fig. 13.** Summary of the ΔSPL spectra when the PA2 plasma actuator is operated at $f_{(input)} = 7$, 8 kHz and $V_{(input)} = 2.4$–4.8 kV at $U = 7.5$–40 ms$^{-1}$. The divisions for zones *A*, *B* and *C* are identical for all the contour maps.

the current PA2 plasma actuator setting. With such a low $\hat{u}/U$ ratio (i.e. low $V_{(input)}$), it is still possible for the PA2 plasma actuator to suppress the vortex shedding based on the indirect modification of the separating shear layer. This mechanism for the suppression of vortex shedding is different with the direct injection of momentum into the wake deficit demonstrated by Nati et al. [17].

### 3.4. Plasma actuator PA3 – spanwise actuations

#### 3.4.1. Characterisation of the plasma jet at quiescent condition

The spanwise plasma array of PA3, as depicted in Fig. 2, is designed to produce the electric winds in the spanwise direction. To examine the induced jet by this particular plasma configuration, a PIV measurement was conducted in an *z*–*y* plane under a quiescent condition. Fig. 14 shows a velocity contour for the plasma-induced vertical velocity $\tilde{v}$ when $V_{(input)} = 3.6$ kV and

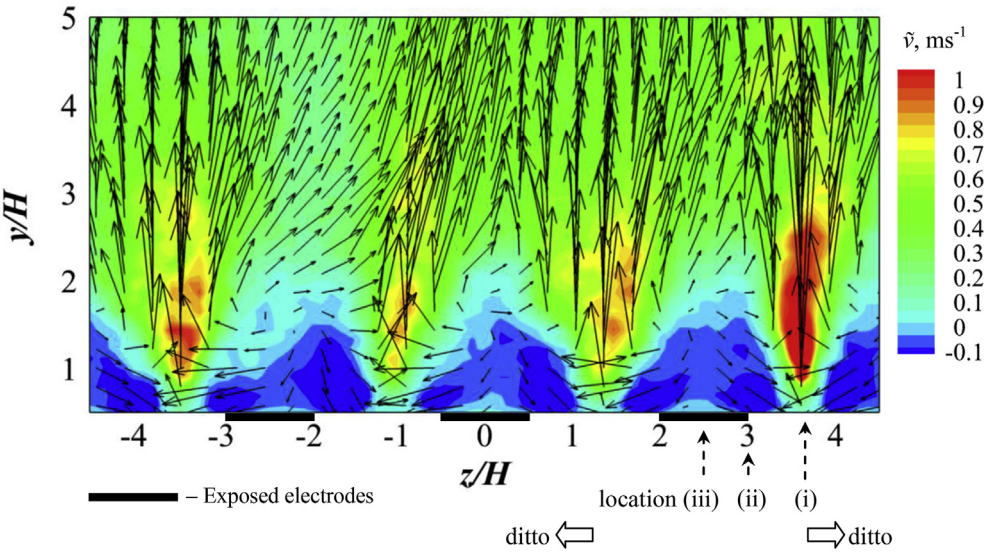


**Fig. 14.** Instantaneous vertical velocity field generated by the PA3 plasma actuator at quiescent condition (i.e. $U = 0$) when $f_{(input)} = 8$ kHz and $V_{(input)} = 3.6$ kV.

$f_{(input)} = 8$ kHz for the plasma actuators. The figure is also superimposed by the full field velocity vectors, which show that each adjacent exposed electrode will ionise the surrounding air and draw the induced flow towards the near wall region. Another body force is created between the exposed electrodes. This body force will create opposite spanwise travelling flows at the near wall region. As shown in Fig. 15, the interaction between the wall-bounded and spanwise airflows will create a streamwise vorticity $\Omega_x$ component of opposite sign between the exposed electrodes. The collision between the opposing spanwise velocity components at the near wall region, however, does not completely result in the cancellation of the spanwise velocity. Rather, the merging of the counter-rotating flow will encourage the production of columns of plasma jet in the positive wall-normal, $y$–direction at the centerline between each pair of the exposed electrodes, i.e. locations (i) correspond to $z/H = \pm 1.25$ and $\pm 3.75$, as shown in Fig. 14.

### 3.4.2. Noise and flow measurements at $U = 7.5\ ms^{-1}$

Although the discussion in Section 3.4.1 is based on the results obtained in the quiescent flow condition, it has been observed that the vertical columns of the plasma-induced jet will not diminish when there is a main flow present. As shown in Fig. 16, when $U = 7.5\ ms^{-1}$, these plasma-generated vortices will be projected into the downstream wake, where the injection of streamwise vorticity $\Omega_x$ into the wake is expected to disrupt the spanwise coherence of the bluntness-induced vortex shedding, and potentially weaken the narrowband tonal noise source. Indeed this has already been demonstrated earlier in Fig. 3 where both the instantaneous spanwise vorticity $\Omega_z$ and POD eigenmodes pertaining to the vortex shedding are significantly suppressed by the PA3 plasma actuators at locations correspond to (i) and (ii).

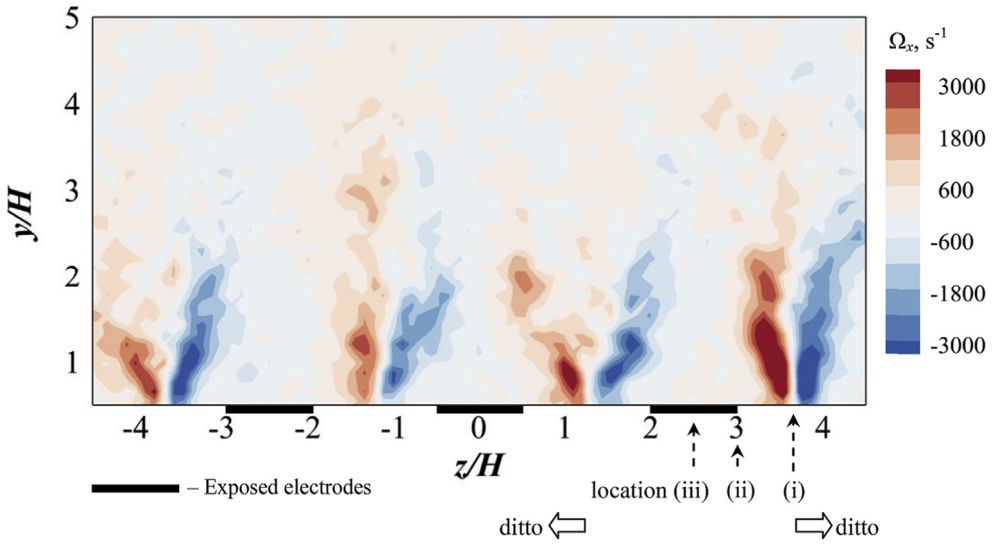


**Fig. 15.** Instantaneous streamwise vorticity field generated by the PA3 plasma actuator at quiescent condition (i.e. $U = 0$) when $f_{(input)} = 8$ kHz and $V_{(input)} = 3.6$ kV.

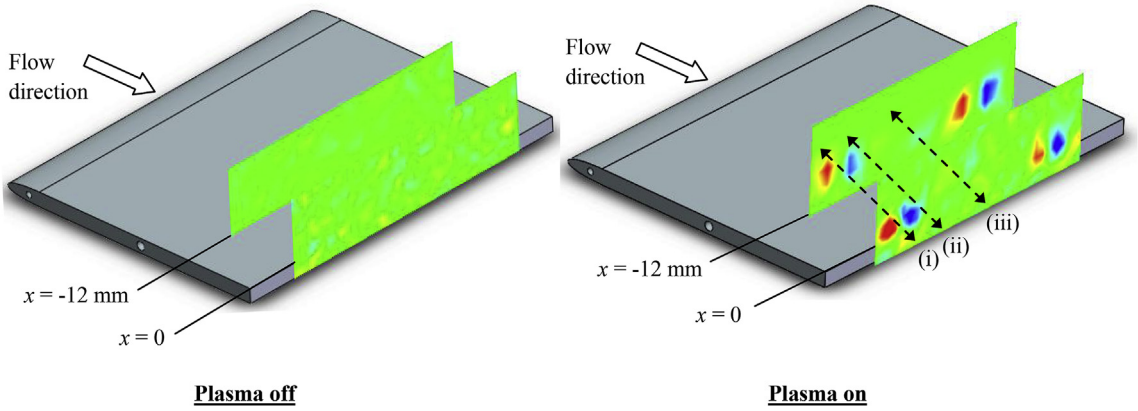


**Fig. 16.** Time-averaged streamwise vorticity fields generated by the PA3 plasma actuator at $U = 7.5\ ms^{-1}$ when $f_{(input)} = 8$ kHz and $V_{(input)} = 3.6$ kV. Drawings are not to scale.

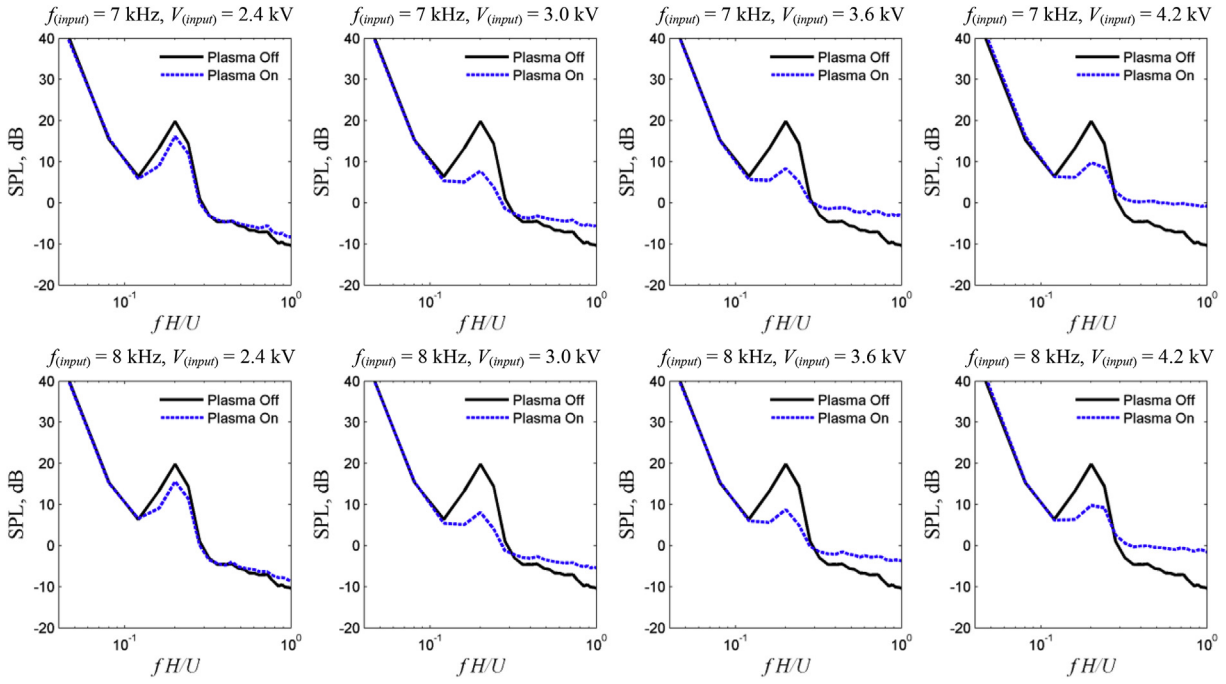


**Fig. 17.** Summary of the SPL spectra when the PA3 plasma actuator is operated at $f_{(input)} = 7$, 8 kHz and $V_{(input)} = 2.4$–4.2 kV at $U = 7.5\ \mathrm{ms}^{-1}$.

The effectiveness of the PA3 plasma actuator in the reduction of the aerodynamic noise is presented in Fig. 17. The figure shows the SPL spectra for the "plasma off" and several PA3 "plasma on" cases at $U = 7.5\ \mathrm{ms}^{-1}$. Similar to the previous presentations, the level of tonal noise reduction is not affected considerably by the $f_{(input)}$. At $V_{(input)} = 2.4$ kV, the level of tonal noise reduction is shown to be $\Delta\mathrm{SPL} = 4$ dB, which is a much better achievement than those by the PA1 and PA2 counterparts under the same $V_{(input)}$ and $U$. When the $V_{(input)}$ is increased to 3.0 kV for the PA3 plasma actuators, the level of tonal noise reduction improves to $\Delta\mathrm{SPL} = 12$ dB. Note that, under the same $V_{(input)}$, the levels of tonal noise reduction by the PA1 and PA2 plasma actuators are only at $\Delta\mathrm{SPL} = 0$ and 3.4 dB, respectively. Based on the results presented thus far, the PA3 (spanwise) plasma actuator seems to be more effective than the PA1 (tangential) and PA2 (downward) plasma actuators in terms of the aerodynamic noise reduction when they are all subjected to the same $V_{(input)}$ and $f_{(input)}$.

However, further increases of the $V_{(input)}$ to 3.6 or 4.2 kV for the PA3 plasma actuators do not result in further improvement of the vortex shedding tonal noise reduction. It is observed that the reduction of the narrowband tonal noise at $0.1 \leq fH/U \leq 0.3$ remains the similar level at $\Delta\mathrm{SPL} = 12$ dB, despite the non-aerodynamic, broadband self-noise level produced by the PA3 plasma actuators at $fH/U > 0.3$ continues to increase with the $V_{(input)}$. It is not yet known whether the magnitude of the PA3 plasma-induced jet velocity will increase as the $V_{(input)}$ increases from 3.0 to 4.2 kV, but it is reasonable to assume that this could be true based on the increased level of the broadband self-noise for the plasma actuator. Since the above settings essentially produce the same level of $\Delta$SPL, the hydrodynamic results measured at $V_{(input)} = 3.6$ kV (i.e. the instantaneous spanwise vorticity $\Omega_z$ and POD modes in Fig. 3, as well as the time-averaged streamwise vorticity $\Omega_x$ in Fig. 16) will be used to analyse the noise results collectively for the $V_{(input)} = 3.0$, 3.6 and 4.2 kV cases.

In Fig. 3, the near complete suppression of the vortex shedding by the PA3 plasma actuators is clearly demonstrated by the POD modes at the $x$–$y$ planes that correspond to the locations: (i) centreline between each pair of the exposed electrodes, and (ii) edge of the exposed electrode. Although the $x$–$y$ plane that corresponds to the (iii) centreline of the exposed electrode was not measured in this study, it is reasonable to assume that certain local vortical structures with strong spanwise vorticity are still present. This is because, as shown in Fig. 16, the plasma-induced streamwise vorticity is only dominant at locations that correspond to (i) and (ii), but not at location (iii). No matter how strong the plasma-induced jet velocity or the streamwise vorticity is produced by the PA3 spanwise plasma actuators in the current setting, there will always be regions (i.e. location iii) where the streamwise vortex shedding is still dominant. In other words, a more effective suppression of the vortex shedding across the whole span is to reduce the spanwise spacing between each successive electrode. However, a reduced spanwise spacing could entail a large capacitance across the whole plasma system, thus potentially reduce the effectiveness of the $V_{(input)}$ with respect to the $\tilde{v}$ produced. This causal relationship would become one of the dilemma in the current design effort to optimise the spanwise plasma actuator concept, which focuses on the minimum expenditure of the $V_{(input)}$ to achieve the maximum reduction in the aerodynamic noise.

In summary, the suppression of the bluntness-induced vortex shedding by the PA3 spanwise plasma actuator involves a different mechanism compared to the PA2 downward plasma actuator. As discussed in Section 3.3.1, the PA2 plasma actuator

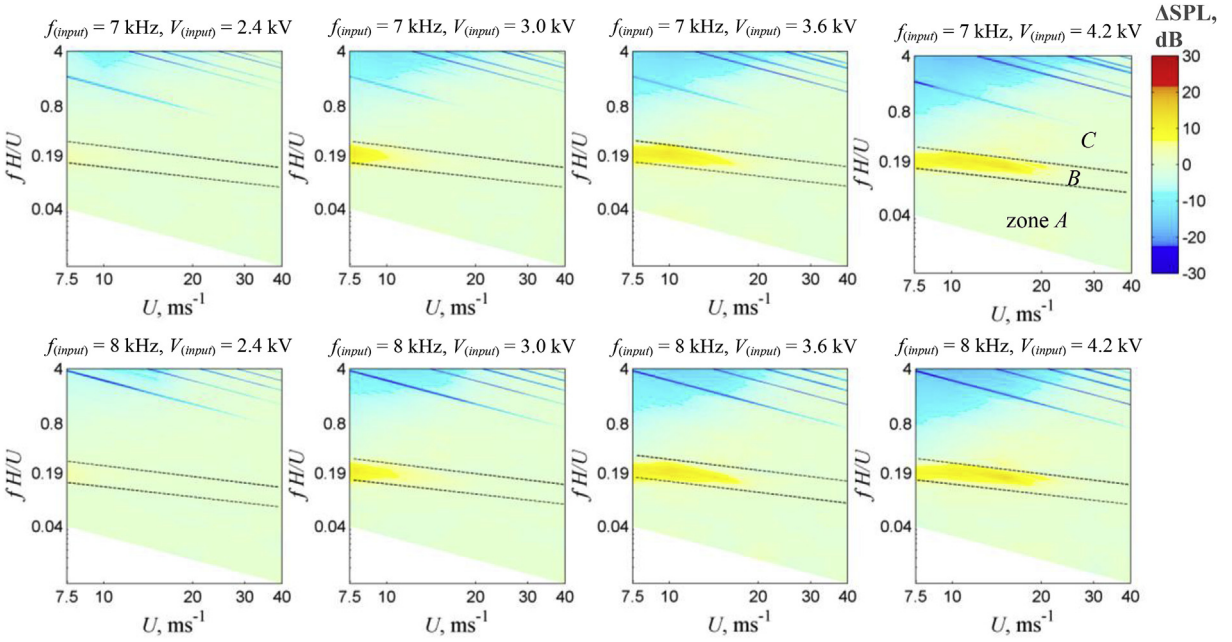


**Fig. 18.** Summary of the ΔSPL spectra when the PA3 plasma actuator is operated at $f_{(input)} = 7$, 8 kHz and $V_{(input)} = 2.4$–4.2 kV at $U = 7.5$–40 ms$^{-1}$. The divisions for zones *A*, *B* and *C* are identical for all the contour maps.

suppresses the vortex shedding based on the mechanisms of indirect modification of the separating shear layer, and the deprivation of the self-sustaining of the wake vortex shedding behind the blunt trailing edge. As a result, the shedding characteristic in the wake, if exists, will be altered considerably (e.g. the alternating POD modes of the vortex structures could become more compact in the wake). The PA3 plasma actuator, on the other hand, injects array of streamwise vorticity into the wake to isolate and compartmentalise the vortex shedding in the spanwise direction. It is interesting to note from Fig. 17 that the acoustic spectra subjected to the PA3 plasma actuators produce a small tonal peak whose frequency remains similar to the baseline, "plasma off" case. This is because the pockets of wake region that are aligned with location (iii), which naturally do not interact with the array of streamwise vortices generated by the PA3 plasma actuators, become a weak source for the tonal noise radiation but nevertheless still retain the characteristic frequency of the original vortex shedding.

### *3.4.3. Tonal noise reduction at higher mean flow velocities*

Based on the acoustic and flow results at $U = 7.5$ ms$^{-1}$, it has been demonstrated that the PA3 (spanwise) plasma actuator is more effective than the PA1 (tangential) and PA2 (downward) plasma actuators in terms of the balance between aerodynamic noise reduction and level of input AC voltage. This section will address whether such proposition remains valid at higher freestream velocity.

Fig. 18 shows the ΔSPL contour maps as a function of $U$ (7.5–40 ms$^{-1}$) and $fH/U$ when subjected to the PA3 plasma actuation at different levels of $V_{(input)}$ and $f_{(input)}$. After the relationship between the $V_{(input)}$ and the plasma-induced vertical velocity $\tilde{v}$ has been established as 0.33 ms$^{-1}$ per kV for the current setting, the results in Fig. 18 can be used to determine the lower-limit of $\tilde{v}/U$ over which the PA3 plasma actuator can still be effective in the suppression of the vortex shedding tonal noise. It is found that the narrowband tonal noise reduction in Zone *B* can still be achieved at $U \approx 21$ ms$^{-1}$ when $V_{(input)} = 4.2$ kV; at $U \approx 18$ ms$^{-1}$ when $V_{(input)} = 3.6$ kV; at $U \approx 14$ ms$^{-1}$ when $V_{(input)} = 3.0$ kV. Therefore the lower-limit for the $\tilde{v}/U$, which represents the minimum ratio of the plasma jet and the freestream velocity for which an effective reduction of the vortex shedding tonal noise can be achieved by the current PA3 spanwise plasma actuator, is about 0.07. This value is lower than the $0.09 \leq \hat{u}/U \leq 0.10$ established earlier for the PA2 downward plasma actuator (see Section 3.3.3).

## 4. Discussion

The dielectric barrier discharge plasma actuators of various configurations have been demonstrated repeatedly in the past by many researchers. Their main focus, however, is for the flow control purpose such as to suppress the flow separation, or even to reduce the turbulent boundary layer skin friction. Although it is known that the far field radiation of the aerodynamic noise is usually a by-product of the separated or turbulent flow, there are still relatively less efforts to address the effect of plasma actuators on the aerodynamic noise problems. This paper attempts to fill this gap by performing a simultaneous flow

and acoustic study on the application of plasma actuators and their reduction of the high amplitude, narrowband vortex shedding tonal noise generated by a flat plate with blunt trailing edge.

Noise measurement of the baseline case, i.e. without turning on the plasma actuators, has consistently shown in the acoustic spectra for a narrowband tonal peak to occur at Strouhal number of 0.24 (based on the plate bluntness) across freestream velocities between 7.5 and 40 $ms^{-1}$. This confirms that the main aerodynamic noise source is the bluntness-induced vortex shedding tonal noise. It is also found that the two excitation frequencies to the plasma actuators investigated here, at 7 and 8 kHz, do not result in significantly different noise reduction performance between them.

Results analysed from an extensive measurement campaign for the PA1 tangential plasma actuator at freestream velocity of 7.5 $ms^{-1}$ show that this particular plasma configuration is not very effective in the suppression of the vortex shedding tonal noise (maximum 1–2 dB reduction only). Although not presented in this paper, further increase of the voltage input greater than 5 kV to the PA1 plasma actuator has been attempted. It was found that although the level of vortex shedding tonal noise reduction can be improved slightly, it is still much lower than the PA2 and PA3 plasma actuators where both can achieve a larger level of aerodynamic noise reduction at a lower voltage input. Despite little advantage in terms of the aerodynamic noise reduction by the PA1 plasma actuator, an interesting aeroacoustic phenomenon has been observed. When subjected to the PA1 plasma actuation, the most dominant mode in the proper orthogonal decomposition reveals that the coherent structures in the wake can become more compact in space. This also indicates that the shedding frequency is now higher. Indeed the corresponding tone frequency of the radiated far field has been shifted to a similar value determined from the vortex shedding hydrodynamic frequency.

The PA2 downward plasma actuator is investigated next. At the quiescent condition (i.e. no main flow present), the PA2 plasma actuator has been shown to produce streamwise jet of about 1.8 $ms^{-1}$. Despite the streamwise plasma jet produced in the current setting is generally less than the reported values in the literature, it is still proven to be very effective in the reduction of the far field vortex shedding tonal noise. For example, 14.5 dB reduction of the tonal noise can be achieved at an input voltage of 4.2 kV at freestream velocity of 7.5 $ms^{-1}$. This is corroborated by the results in the proper orthogonal decomposition where the most dominant modes pertaining to the coherent structures have been completely suppressed. Examination of the wake velocity profile subjected to the same PA2 plasma actuator also indicates that both the mean and fluctuating components of the drag coefficient can be reduced significantly.

Further examination of the near wake velocity profiles and the 2D vorticity contour in the $x$–$y$ plane suggests that the reason the PA2 plasma actuator can be so effective in the suppression of the wake vortex shedding and the reduction of far field tonal noise is not related to the direct momentum injection to the wake deficit *per se*. This is because the plasma-induced jet will decay very quickly from the blunt trailing edge when there is main flow present. Rather, the streamwise jet produced by the plasma actuator acts to inhibit the interaction between the upper and lower separating shear layers, and to delay the formation of the vortex shedding until a further downstream location. This is confirmed by the far wake hot wire measurement, where the fluctuating velocity power spectral density shows a reduction at the Strouhal number of 0.23, which is similar to the acoustical Strouhal number for the far field tone peak. It is also observed that the broadband component of the fluctuating velocity power spectral density is reduced at higher frequency when the PA2 plasma actuator is turned on. To summarise, the downward actuation of the PA2 plasma actuator is very effective in the suppression of the bluntness-induced vortex shedding tonal noise even operated at a relatively low voltage input. Furthermore, the streamwise plasma jet magnitude only requires about 9–10% of the freestream velocity to be sufficient to achieve an effective reduction of the vortex shedding tonal noise.

For the PA3 spanwise plasma actuator, the flow field measurement by the PIV confirms that the near wall spanwise plasma jet, when coupled with the wall-normal jet due to entrainment, can produce multiple arrays of counter-rotating streamwise vortices. When there is a mean flow of 7.5 $ms^{-1}$ present, these plasma-generated vortices will be projected into the downstream wake, which then isolate and compartmentalise the bluntness-induced vortex shedding across the spanwise direction. These interactions will ultimately cause a weakening of the tonal noise source in the wake. Interestingly, this particular plasma configuration is even more effective than the PA2 plasma actuator in terms of the balance between the level of narrowband tonal noise reduction and the voltage input. For example, using a relatively low input voltage of 3.0 kV for the PA3 plasma actuator will achieve a 12 dB tonal noise reduction compared to the 3.4 dB reduction by the PA2 plasma actuator. However, further increases of the input voltage to the PA3 plasma actuator to 4.0 or 4.2 kV do not result in further reduction of the tonal noise level. The reason behind this will be explained in the next paragraph.

The large reduction of the far field tonal noise is corroborated by the absence of discernible coherent modes in the proper orthogonal decomposition of the flow fields between the exposed electrodes (i.e. locations i and ii as depicted in Fig. 2). However, the flow field downstream of each exposed electrode (i.e. location iii) can be isolated by the streamwise vortices originally produced by the plasma winds. Therefore it is expected that the local spanwise vorticity fields pertaining to the vortex shedding will remain relatively intact, and is still capable of radiating weaker level of tonal noise collectively into the far field. In the current study, the spanwise spacing between the exposed electrodes is fixed at one particular value, which might not be the most optimised setting. In other words, one should also focus on minimising the spanwise spacing between the exposed electrodes (or minimising the width of the exposed electrodes) to allow a more closely-packed array of streamwise vortices to be generated. This will potentially enhance the receptivity of the PA3 plasma actuator to the voltage input, and continue to achieve further level of aerodynamic noise reduction. Finally, it has been shown that the induced-jet $\tilde{v}$ generated by the PA3 plasma actuator only needs about 7% of the freestream velocity to achieve an effective reduction of the vortex shedding tonal noise. This is lower than the 9–10% needed for a PA2 plasma actuator.

## 5. Conclusion

This paper investigates three DBD plasma actuator configurations, namely the tangential actuation (PA1), downward actuation (PA2) and spanwise actuation (PA3), and their effectiveness in the suppression of vortex shedding and tonal noise radiation from a flat plate with blunt trailing edge. The PA1 and PA2 plasma actuators both produce two-dimensional air jet to interact with the downstream wake vortex shedding. However, the PA3 plasma actuator produces array of counter-rotating streamwise vortices in the same manner as the vortex generators. The input AC voltages to these plasma actuators were kept relatively low at $< 5$ kV, which aligns with the trend of developing plasma flow control devices that do not need very high voltage input, as well as ensuring that the broadband self-noise generated by the plasma actuators remains less critical.

The experiment was performed in an aeroacoustic facility where both the noise and flow measurements were conducted *in situ*. Whilst the PA1 plasma actuator is not very effective in the suppression of vortex shedding tonal noise (maximum 1–2 dB reduction), it was found from the proper orthogonal decomposition analysis that the spatial distribution of the wake coherent modes become more compact. This results in a shift of the tone frequency to a higher value. The PA2 plasma actuator, on the other hand, can suppress the vortex shedding tonal noise almost completely at the tone frequency (reduction of 14.5 dB at input voltage of 4.2 kV). The mechanism is related to the induced plasma jet acting as a barrier to inhibit the interaction between the upper and lower separating shear layers, and to delay the formation of the vortex shedding. This is a different mechanism compared with the direct injection of flow momentum into the wake deficit, which would otherwise require high input AC voltage. The PA3 plasma actuator can project array of streamwise vortices into the wake, compartmentalise the otherwise dominant spanwise vorticity field, and inhibit the formation of vortex shedding and reduce the level of tonal noise radiation. The PA3 plasma actuator demonstrates a more superior tonal noise reduction capability at low input voltage (about 12 dB reduction at 3.0 kV), and has a good potential to eventually become a more versatile aerodynamic noise control device.

## Acknowledgments

This work is supported by the EPSRC in the UK through research grant No. EP/K002309/1. The PhD studentship for the first author is funded by the Iraqi Cultural Attaché in London. The first and second authors would like to thank Mr. Till Biedermann and Professor Frank Kameier from the Düsseldorf University of Applied Sciences for their generosity to loan the PIV system to Brunel University.

## Appendix A. Supplementary data

Supplementary data related to this article can be found at https://doi.org/10.1016/j.jsv.2018.08.029.

## References

[1] H. Choi, W. Jeon, J. Kim, Control of flow over a bluff body, Annu. Rev. Fluid Mech. 40 (2008) 113.
[2] S. Bailey, G. Kopp, R. Martinuzzi, Vortex shedding from a square cylinder near a wall, J. Turbul. 3 (2002) 1.
[3] Y. Jodai, Y. Takahashi, M. Ichimiya, The effects of splitter plates on turbulent boundary layer on a long flat plate near the trailing edge, J. Fluid Eng- T. ASME 130 (2008), 051103 (7 pages).
[4] S. Ozono, Flow control of vortex shedding by a short splitter plate asymmetrically arranged downstream of a cylinder, Phys. Fluids 11 (1999) 2928.
[5] H. Akilli, B. Sahin, N.F. Tumen, Suppression of vortex shedding of circular cylinder in shallow water by a splitter plate, Flow Meas. Instrum. 16 (2005) 211.
[6] A. Roshko, On the wake and drag of bluff bodies, J. Aeronaut. Sci. 22 (1995) 124.
[7] H. Liu, M. Azarpeyvand, J. Wei, Z. Qu, Tandem cylinder aerodynamic sound control using porous coating, J. Sound Vib. 334 (2015) 190.
[8] Y.J. Chen, C.P. Shao, Suppression of vortex shedding from a rectangular cylinder at low Reynolds numbers, J. Fluid Struct. 43 (2013) 15.
[9] L. Henning, R. King, Drag reduction by closed-loop control of a separated flow over a bluff body with a blunt trailing edge, in: Proceedings of the 44th IEEE Conference on Decision and Control, 2005, p. 494.
[10] O. Stalnov, V. Palei, I. Fono, K. Cohen, A. Seifert, Experimental estimation of a D-shaped cylinder wake using body-mounted sensors, Exp. Fluids 42 (2007) 531.
[11] M.L. Post, T.C. Corke, Separation control using plasma actuators: dynamic stall vortex control on oscillating airfoil, AIAA J. 44 (2006) 3125.
[12] Y. Akansu, F. Karakaya, A. Şanlısoy, Active control of flow around NACA 0015 airfoil by using DBD plasma actuator, Eur. Phys. J. Conf. 45 (2013) 01008 (7 pages).
[13] R.D. Whalley, K.S. Choi, Turbulent boundary-layer control with plasma spanwise travelling waves, Exp. Fluids 55 (2014) 1796.
[14] X. Huang, X. Zhang, Streamwise and spanwise plasma actuators for flow-induced cavity noise control, Phys. Fluids 20 (2008), 037101 (10 pages).
[15] F.O. Thomas, A. Kozlov, T.C. Corke, Plasma actuators for cylinder flow control and noise reduction, AIAA J. 46 (2008) 1921.
[16] X. Huang, X. Zhang, Y. Li, Broadband flow-induced sound control using plasma actuators, J. Sound Vib. 329 (2010) 2477.
[17] G. Nati, M. Kotsonis, S. Ghaemi, F. Scarano, Control of vortex shedding from a blunt trailing edge using plasma actuators, Exp. Therm. Fluid Sci. 46 (2013) 199.
[18] L. Tonks, I. Langmuir, Oscillations in ionized gases, Phys. Rev. 33 (1929) 195.
[19] G. Berkooz, P. Holmes, J.L. Lumley, The proper orthogonal decomposition in the analysis of turbulent flows, Annu. Rev. Fluid Mech. 25 (1993) 539.
[20] R.A. Antonia, S. Rajagopalan, Determination of drag of a circular cylinder, AIAA J. 28 (1990) 1833.